Finetuning ERK activity enables most somatic cells to reprogram into pluripotency

Qiao Wu[1,2], Jian Zhang[1,2], Xiao Hu[1,2], Bruna Mafra de Faria[1,2], Steven Maxwell Scalf[1,2], Kutay Karatepe[1,2], Ananda L Roy[3] and Shangqin Guo[1,2,*]

[1]Department of Cell Biology, Yale University, New Haven, CT, 06520, USA

[2]Yale Stem Cell Center, Yale University, New Haven, CT, 06520, USA

[3]National Institutes of Health, Laboratory of Molecular Biology and Immunology, Biomedical Research Center, National Institute on Aging, Baltimore, MD, USA

[*]Correspondence should be addressed to S.G. Email: shangqin.guo@yale.edu

Address: 10 Amistad St. Room 131H, New Haven, CT 06520

Phone: 203-737-6411, fax: 203-785-4305

Abstract

Somatic cell reprogramming is a stochastic process typically resulting in only a small fraction of cells successfully converting into induced pluripotent stem cells (iPSCs). The molecular and cellular basis underlying this stochasticity remains elusive. Here we demonstrate that this stochasticity can be largely eliminated when extracellular signal-regulated kinase (ERK) activity is tuned within a narrow range by using the MEK inhibitor at one tenth the concentration in the 2i media. Without pharmacologic inhibition, cells tune ERK activity by TFII-IΔ, a multifunctional transcription factor that binds to and mediates ERK's nuclear activation. We find TFII-IΔ to be an actin-binding protein. ERK activity is partially inhibited as TFII-IΔ binds to actin which accumulates inside the nucleus of cells undergoing morphological remodeling. Manipulating actin's ability to accumulate inside the nucleus alters reprogramming amenability as well cell height. Actin-TFII-IΔ drive cell height to go above the minimal height required for pluripotency (10 μm). This work uncovers a mechanistic couple between cell morphology and identity, providing convenient practices to massively increase reprogramming efficiency.

Introduction

Pluripotent stem cells (induced pluripotent stem cells, iPSC; embryonic stem cells, ESC) display stereotypic cell/colony morphology, informing the day-to-day quality assessment of the cultures. Naïve iPSC/ESC colonies display "dome-shaped" morphology, loss of which indicates exit from naïve pluripotency [1,2]. Even though cell morphology constitutes an integral aspect of a cell's identity, it is unclear how morphology is molecularly coupled to enable specific identity.

Cell morphology is largely determined by the actin cytoskeleton, dynamic proteinaceous structures consisted of monomeric G-actin and polymeric F-actin [3,4]. Actin dynamics is further modified by many actin binding proteins, such as nucleators, crosslinkers, branchers, as well as cross talkers with the other components of the cytoskeleton [5-8]. Actins, together with myosins, form molecular motors that convert chemical energy into mechanical energy. Therefore, the actomyosin system is central to transducing and interpreting the mechanical signals between the cell and its environment [9-13]. Actin is one of the most abundant cellular proteins, with the majority of the actin pool known to be present in the cytoplasm of most cell types [14,15]. The presence of a small pool of nuclear actin has been long considered an impurity or artifact until relatively recently [16-26]. Here, we report that mouse pluripotent stem cells allocate a significant portion (>50%) of their actin pool into the nucleus; allocating more actin into the nucleus facilitates cell morphological changes favoring pluripotency.

TFII-I (encoded by *Gtf2i*) is a multifunctional transcription factor with several alternatively spliced isoforms involved in signal-induced gene regulation [27-32]. We discovered that the delta isoform of TFII-I (TFII-IΔ), previously reported to undergo cytoplasmic and nucleus shuttling [33], to be highly expressed in cells transitioning into pluripotency. Nuclear actin promotes reprogramming by binding to TFII-IΔ, thereby limiting ERK's activation mediated by TFII-IΔ. Mimicking this mild ERK inhibition pharmacologically eliminates the stochasticity in Yamanaka reprogramming, resulting in the reactivation of pluripotency from most fibroblasts.

Results

More actin inside the nucleus favors pluripotency

In addition to being a major component of the cytoskeleton, actin dynamics participates in transducing mechanical signals, in large part by binding to and inhibiting the mechanosensitive transcriptional co-activator MKL1 [9,34-36]. Together with its binding partner Serum Response Factor (SRF), MKL1 drives the expression of hundreds of genes involved in contractility and adhesion. A truncated MKL1 lacking the actin binding domains is constitutively active (caMKL1), which potently arrests somatic cell reprogramming into pluripotency [37]. The arrested reprogramming can be rescued by genetic or pharmacologic inhibitors of actomyosin contractility. In addition to the rescuers reported in Hu et al. [37], we found that shRNAs targeting *Xpo6,* the exportin for nuclear actin, similarly rescued the caMKL1-blocked cells into pluripotency (Fig. S1a-c). These results suggest that failure to activate pluripotency could be related to insufficient actin in the nucleus. Consistent with this interpretation, a significant portion of the actin pool is found in the nucleus of ESC and iPSC (Fig. 1a). Furthermore, more actin becomes allocated into the nucleus during somatic cell reprogramming into pluripotency, with the somatic (hematopoietic) cells displaying predominantly cytoplasmic actin (Fig. 1b, Fig. S1d).

To test whether allocating more actin into the nucleus promotes somatic cell reprogramming into pluripotency, we transduced Mouse Embryonic Fibroblasts (MEFs) derived from doxycycline (Dox) inducible Oct4/Klf4/Sox2/Myc (OKSM) mice expressing the Oct4:GFP reporter ($R26^{rtTA}$;$Col1a1^{4F2A}$;$Oct4^{GFP}$) [38,39], with a retroviral construct encoding β-actin, tagged on the N-terminus with a nuclear localization signal (NLS) and FLAG epitope (Fig. 1c). Empty vector (EV)

or wild type (WT) β-actin were used as controls. The presence of exogenously expressed actin was confirmed by immunofluorescence (IF) against FLAG (Fig. 1d). In cells expressing the WT β-actin, most FLAG signals localized to the cytoplasm, confirming actin's predominant cytoplasmic localization. In contrast, FLAG signal was enriched in the nucleus of cells expressing NLS-actin. The nuclear FLAG signals appeared as elaborate networks (Fig. 1d, Movie S1), suggesting that the NLS-actin is involved in F:G (filamentous and globular actin), dynamics and crosslinking/branching with the endogenous actin. Of note, cytoplasmic FLAG signals were also detected in cells expressing NLS-actin, likely reflecting actin's strong tendency toward cytoplasmic localization despite the NLS, with a key determining factor becoming clear later in this study. The overexpression level is mild, estimated to be ~1% of the endogenous actin (Fig. 1e, S1e). Reprogrammable MEF expressing these constructs were treated with Dox to induce OKSM. Strikingly, the number of alkaline phosphatase positive (AP+) or Oct4:GFP positive colonies were greatly increased by NLS-actin expression, while no difference was shown by cells expressing WT β-actin (Fig. 1f-h). To determine whether F:G dynamics is required for NLS-actin to promote reprogramming, we expressed point mutants NLS-actin^{G13R} and NLS-actin^{S14C}, defective in polymerization or depolymerization, respectively [40] (Fig. 1f-h, S1f, Movies S2,3). Neither mutants increased the number of AP+ or Oct4:GFP+ colonies. Therefore, concentrating F:G competent actin inside the nucleus promotes pluripotency induction from mammalian somatic cells, contrasting the findings in frog oocytes in which polymerized nuclear actin was more functional [41].

Besides the increased numbers of AP+ and Oct4:GFP+ colonies, the colonies arising from NLS-actin expressing cells had sharp borders and were light reflective, displaying typical dome shaped morphology on day 15 (Fig. 1i). In contrast, many of the colonies in EV control reprogramming cultures had Oct4:GFP+ cells diffused/mixed within flatter colonies. Further, Oct4:GFP was brighter when NLS-actin was expressed, as determined by flow cytometry (Fig. 1j-l). Over time, the Oct4:GFP+ cells from EV cultures matured and acquired an intensity similar to those expressing NLS-actin, while the %Oct4:GFP+ in the latter expanded. Lastly, NLS-actin promoted reprogramming is not limited to MEFs, as NLS-actin similarly promoted reprogramming of hematopoietic cells (Fig. S1g-i). Taken together, NLS-actin promotes pluripotency induction from somatic cells by Yamanaka factors.

NLS-actin promotes somatic cell reprogramming defying known mechanisms

To understand how NLS-actin facilitates pluripotency activation, we began by comparing the transcriptomes of MEFs expressing NLS-actin, WT β-actin and EV (Fig. 2a,b, Table S1). In the absence of Yamanaka factor expression (Vehicle), neither actin constructs caused substantial transcriptomic changes. 4 days of Yamanaka factor expression (Dox) led to changes in thousands of genes irrespective of the co-expressed actin constructs (Fig. 2b), as expected. We therefore focused on the transcriptomic differences in reprogramming cells co-expressing either actin constructs, or as compared to EV controls. WT β-actin and NLS-actin similarly reduced SRF target genes as assessed by Gene Set Enrichment Analysis (GSEA) [42,43] (Fig. 2c,d, S2a**),** confirming actin's known effects in inhibiting MKL1/SRF. Despite their similar inhibition of SRF targets, GSEA revealed that NLS-actin expressing cells more resemble pre-iPSCs, as defined by Polo et al. [44] relative to those expressing WT β-actin (Fig. 2e). Since many SRF targets are typical mesenchymal genes, the similar inhibition of SRF targets by both actin constructs argues against the notion that antagonizing mesenchymal identity is how NLS-actin promotes reprogramming (Table S1). Gene Ontology (GO) analysis of the 158 up- and 300 down-regulated (differentially expressed genes) DEGs (Fig. 2b) between the actin constructs only enriched for "structural constituent of ribosome", "pre-mRNA intronic binding" and cadherin

based adhesion (Table S2), yielding little insights into the mechanism how NLS-actin promotes pluripotency.

Even after 8 days of factor induction, when increased H3K4me3 marks at pluripotency genes became prominent in NLS-actin expressing cells (Fig. S2b,c), cells expressing different constructs displayed no difference in cell cycle, bulk transcriptional activity or DNA damage (Fig. S2d-f), all processes in which nuclear actin have been reported to function [19,45-53]. As cell extrinsic signals such as secreted factors in the medium could influence reprogramming [54], we next compared cells within the same culture using mCherry fluorescence to distinguish cells with or without NLS-actin (Fig. 2f-j). At day 10 when Oct4:GFP+ cells began to emerge (0.55% Oct4:GFP+), the mCherry+ cells were enriched for iPSC genes as compared to the mCherry- cells from the same culture (Fig. 2g,h). Robust Oct4:GFP+ cells (38.8%) emerged on day 14, of which about 25.1% were mCherry- (Fig. 2i). On day 14, among the Oct4:GFP- population, the mCherry+ cells were still enriched for iPSC genes as compared to the mCherry- counterparts (Fig. 2j, left). In contrast, day 14 Oct4:GFP+/mCherry+ cells were less similar to iPSCs as compared to the Oct4:GFP+/mCherry- cells, consistent with the latter being mature iPSCs that have silenced the retroviral construct (Fig. 2j, right). When all cell states throughout the reprogramming time course were compared by CellNet analysis [55] (Fig. 2k, S2g), it confirmed that reprogramming was initiated from fibroblasts, went through intermediate states and ended with a cell state highly similar to ESC. However, CellNet analysis could not even detect a more advanced cell state toward pluripotency at day 10 in NLS-actin expressing cells (Fig. 2k, S2g), Therefore, NLS-actin's surprising pro-reprogramming effect remains difficult to explain through its known modes of action.

Gtf2i/TFII-I is required for NLS-actin to promote reprogramming

To understand how nuclear actin promotes somatic cell reprogramming, we determined the nuclear actin interactome in the reprogramming intermediates by co-immunoprecipitation (Co-IP) with FLAG antibody followed by mass spectrometry (Fig. S3a). Silver stain of the nuclear protein precipitates from WT β-actin and NLS-actin expressing cells detected two prominent bands of 42 KD and 250 KD, corresponding to actin and Myh9/10, respectively, and confirmed by protein-specific antibodies (Fig. 3a,b). Other abundant nuclear proteins such as histone H3 was not enriched, confirming the specificity of our approach. A total of 122 proteins with at least 2 unique peptides in the WT β-actin or NLS-actin samples were recovered (Table S3). These 122 candidates include 38 known actin-binding proteins, 76 known RNA binding proteins and 22 known DNA binding proteins (Fig. 3c). The large number of known DNA/RNA binding proteins is consistent with their nuclear enriched expression. We envisioned that this nuclear actin interactome contain mediators for NLS-actin's pro-reprogramming function.

We next constructed a custom guide RNA (gRNA) library to pinpoint the candidate(s) that mediate NLS-actin's pro-reprogramming function. If a specific gene is required for NLS-actin to promote reprogramming, NLS-actin+ cells expressing gRNAs targeting that gene should not reprogram, resulting in depletion of such gRNAs relative to the other gRNAs in the library, quantifiable by sequencing. This nuclear actin interactor targeting (NAIT) library contains 528 gRNAs against the 122 candidates plus 10 additional control genes, with 4 gRNAs per gene (Table S4). The pooled sgRNA library, co-expressing blue fluorescence protein (BFP), was transduced into Cas9 expressing reprogrammable MEFs (Fig. 3d). BFP+ cells were then transduced with NLS-actin/mCherry and genomic DNA was harvest as input DNA. After Dox induction, mCherry+ and mCherry- cells were sorted to provide at least 150x coverage, sufficient to detect these reprogramming cells which had an efficiency of ~7.5% (Fig. 1h). The abundance of individual gRNAs in the mCherry+/- cells was quantified by sequencing starting at

179 day 4 and compared against the input DNA [56,57]. This analysis revealed that multiple gRNAs
180 targeting *Gtf2i* (encoding TFII-I) were the most depleted in the NLS-actin expressing cells (Fig.
181 3e, S3b,c, Table S4). We validated that TFII-I protein is indeed precipitated by NLS-actin (Fig.
182 S3d), and IF detected prominent TFII-I signal on the fibrous nuclear actin network (Fig. S3e,f).
183
184 To independently validate the functional importance of *Gtf2i* in mediating NLS-actin's pro-
185 reprogramming effect, we designed three shRNAs against *Gtf2i* and confirmed their knockdown
186 in reprogrammable MEF (Fig. 3f). Of note, *Gtf2i* was previously identified in a genome wide
187 screen as a reprogramming barrier during the transitional stage [58]. In the non NLS-actin
188 expressing cells, *Gtf2i* shRNAs increased colony numbers by ~2 fold (Fig. 3g), similar to the
189 report by Yang et al. [58]. In comparison, NLS-actin caused increase in colony numbers was more
190 pronounced (Fig. 3g, S3g,h). Importantly, NLS-actin-mediated increase in colony numbers was
191 abolished by the *Gtf2i* shRNAs. The effects could be seen with all three individual *Gtf2i* shRNAs
192 (Fig. 3g, S3g,h). In subsequent experiments, these shRNAs were pooled which yielded similar
193 knockdown efficiency (Fig. 3h). Consistent with the increase in Oct4:GFP+ colony numbers,
194 *Gtf2i* targeting shRNAs led to brighter Oct4:GFP in EV control cells (Fig. 3i-l). Strikingly, no
195 Oct4:GFP+ colonies were present in NLS-actin expressing cells with *Gtf2i* knockdown (KD).
196 Further, such colonies appeared spread or flat (Fig. 3i, bottom right). Thus, NLS-actin depends
197 on *Gtf2i*/TFII-I to promote reprogramming.
198
199 **The delta isoform of TFII-I, TFII-IΔ, mediates NLS-actin's pro-reprogramming effect**
200 TFII-I is highly conserved between human and mouse and has several alternatively spliced
201 isoforms [59,60]. Two of the abundant isoforms, Δ and β, are detected in most cell types, including
202 fibroblasts (Fig. 4a). Of note, *Gtf2i* mRNA reads mapping to this alternative region were
203 abundant during reprogramming (Fig. 4a, boxed region). As this region is involved in generating
204 the Δ and β isoforms, these results suggest that TFII-I isoforms could be differentially expressed
205 during reprogramming, even though the mRNA reads of the entire *Gtf2i* gene remains similar
206 (Fig. S4a). To better resolve the expression of these isoforms, we designed primers that span
207 the alternatively utilized exons (Fig. 4a, black arrows). The transcripts detected by these primers
208 decreased in the reprogramming intermediates, while the relative portion of Δ increased (Fig.
209 4b,c). Together, these results suggest that specific *Gtf2i* isoform, the Δ isoform, might be the
210 relevant one in mediating NLS-actin promoted pluripotency activation. Indeed, a larger TFII-I
211 protein band dominated in MEF, while iPSC expressed a faster-migrating species, consistent
212 with their expression of the β and Δ isoforms, respectively (Fig. 4d) [33]. Lastly, the expression of
213 these isoforms in mature iPSC and ESC is sensitive to cell plating density (Fig. 4e): the Δ
214 isoform dominates at high density, while β becomes more abundant at low density (Fig. 4e).
215 These results echo our previous findings that higher cell density favors pluripotency [54].
216 Together, these results suggest Δ-specific biology during reprogramming.
217
218 To further test the isoform-specific roles, we designed two additional shRNAs targeting *exon 12*
219 (Fig. 4a, orange bars), which is absent in *Gtf2iΔ*, while the shRNAs shown earlier (Fig. 3f-k,
220 S3g,h) targeted both *Δ* and *β* isoforms (Fig. 4a, three black bars) and will be referred to as the
221 *Δ/β* dual targeting shRNAs from here on. Indeed, either *β*-specific or *Δ/β* dual targeting shRNAs
222 efficiently reduced TFII-I protein in the initial MEF, which predominantly express the larger β
223 isoform (Fig. 4f, S4b). In contrast, only the *Δ/β* dual targeting shRNAs reduced the protein in
224 later reprogramming cells (day 12), which expressed the smaller Δ isoform (Fig. 4f, Fig. S4b).
225 Importantly, the *β*-specific shRNAs did not change the number of AP+ or Oct4:GFP+ colonies in
226 NLS-actin expressing cells, contrasting the situation with *Δ/β* dual targeting shRNAs (Fig. S4c-e,
227 compare to Fig. 3f-l and Fig. S3g,h). Consistent with the unchanged colony numbers, *β*-specific
228 shRNAs did not affect NLS-actin promoted Oct4:GFP intensity (Fig. 4g-j). These results further

229 support that TFII-IΔ is the relevant isoform under our experimental conditions. From here on, we
230 focused on how TFII-IΔ functions in reprogramming.
231
232 **Inhibiting TFII-IΔ while co-expressing NLS-actin reduces pERK to a level not permissive**
233 **for reprogramming**
234 Next, we co-expressed TFII-IΔ directly with or without NLS-actin in reprogramming MEFs (Fig.
235 5a-c). Consistent with its role in mediating NLS-actin's effect, TFII-IΔ co-expression potentiated
236 NLS-actin promoted reprogramming. Remarkably, a tyrosine to phenylalanine point mutant TFII-
237 IΔ^{Y248F} abolished this potentiation effect. Since this TFII-IΔ^{Y248F} mutant was reported to be
238 defective in binding ERK [30], we examined pERK binding to TFII-IΔ in the reprogramming
239 intermediates by co-IP. Indeed, pERK binding to TFII-IΔ^{Y248F} was significantly reduced as
240 compared to WT TFII-IΔ, particularly in NLS-actin expressing cells (Fig. 5d). These results
241 suggest that effect of NLS-actin-TFII-IΔ on reprogramming could be mediated through
242 regulating ERK activity.
243
244 TFII-IΔ is an atypical transcription factor in that it can shuttle between the cytoplasm and the
245 nucleus. When TFII-IΔ translocates into the nucleus upon growth-factor signaling, it imports
246 pERK leading to the activation of ERK target genes such as *c-fos* [33]. Given ERK's well
247 established function in regulating pluripotency [61-68], and iPSC have low pERK (Fig. 5e), we
248 examined whether ERK activity is affected by NLS-actin and/or TFII-IΔ. As indicated by the live
249 cell ERK-KTR reporter [69,70], NLS-actin expression dampened serum stimulated ERK activation
250 (Fig. 5f). Specifically, ERK remained active at least 40 minutes after serum stimulation in EV
251 control cells; in contrast, ERK became inactivated in NLS-actin expressing cells as soon as
252 serum was washed out. We next examined the endogenous ERK activity in reprogramming
253 MEFs by western blotting for pERK. Consistent with the results by the ERK-KTR reporter, pERK
254 level was reduced in NLS-actin expressing cells (Fig. 5g,h). Furthermore, Δ/β dual targeting
255 shRNAs also reduced pERK levels, consistent with its reported role in mediating pERK's
256 nuclear activation [33]. Thus, either NLS-actin expression or Δ/β dual targeting shRNAs each
257 reduced ERK activity and promoted reprogramming. However, while the lowest pERK level
258 occurs with simultaneous NLS-actin expression and Δ/β KD, such a condition became
259 incompatible with reprogramming (Fig. 5g-h, also refer to Fig. 4g-j, 3f-k). We interpreted these
260 results to mean that even though lowering ERK activity favors pluripotency, pluripotency may
261 need to arise within a narrow range of ERK activity; lowering it further beyond this range would
262 again inhibit reprogramming. Such an interpretation is consistent with a model where the TFII-IΔ
263 pool for activating ERK is constrained by binding to actin. We tested this possibility by
264 fluorescence recovery after photobleaching (FRAP) using TFII-IΔ-GFP fusion protein. This
265 confirmed that NLS-actin indeed rendered TFII-IΔ-GFP slower to recover after photobleaching
266 (Fig. S5a). Taken together, TFII-IΔ tunes ERK activity to promote reprogramming, a process
267 that became unmasked by NLS-actin expression; as the TFII-IΔ pool bound to actin becomes
268 compromised for ERK activation, further reducing TFII-IΔ by sgRNAs or shRNAs abolishes
269 reprogramming.
270
271 **Mild ERK inhibition by chemical inhibitors promotes reprogramming from most**
272 **fibroblasts**
273 The ERK tuning model predicts that pluripotency would be effectively induced if ERK activity is
274 tuned pharmacologically. We therefore treated reprogrammable MEF with Dox in the presence
275 of a well validated MEK inhibitor, PD032591, ranging from 0.05 μM to 1 μM, a staple of the 2i
276 media for cultivating naïve ESC [65]. Progression toward pluripotency was monitored by flow
277 cytometry for %Oct4:GFP+ (Fig. 6a). Strikingly, in the presence of 0.1 μM of PD032591, >60%
278 of all cells became Oct4:GFP+ by 13 days and ~80% cells were Oct4:GFP+ on day 21 (Fig.

279 S6a,b). In contrast, the %Oct4:GFP+ remained low throughout in 0.05 or 0.25 μM of PD032591.
280 The effect of mild ERK inhibition was confirmed by western blotting for pERK (Fig. 6b,c). Of
281 note, there was a sharp drop in pERK level between reprogramming day 4 and 7. While 0.1 μM
282 PD0325901 had no discernible inhibition of pERK on day 4, the inhibition became clear on day
283 7. We repeated this mild inhibition by another ERK inhibitor, U0126. Low dose U0126 also
284 significantly increased the %Oct4:GFP+ cells, albeit to a lesser extent than PD0325901 (Fig.
285 S6c-f). Therefore, somatic cell reprogramming into pluripotency is greatly increased when ERK
286 activity is tuned within a narrow range. We interpreted these results to indicate that the
287 probability of a given cell to tune their ERK activity within this range is low (i.e. stochastic); when
288 enforced pharmacologically, reprogramming into pluripotency is no longer rare and could occur
289 in most cells (Fig. S6g). Consistently, 0.1 μM PD0325901 became ineffective in cells that
290 already express NLS-actin or have TFII-IΔ KD (Fig. 6d-f). Therefore, excessive ERK inhibition
291 by combining molecular and chemical inhibitors yields a cell state that is no longer permissive
292 for pluripotency initiation.
293
294 With the insights that mild reduction in ERK activity could be how NLS-actin promotes
295 reprogramming, we re-examined the transcriptomes of reprogramming MEF expressing the
296 actin constructs (Fig. 2b). To this end, we found that a small subset of ERK target genes,
297 originally defined using optogenetically controlled ERK [71] (ERK^{pulse}), were significantly down-
298 regulated in NLS-actin expressing cells (Fig. 6g); most other ERK targets did not change with
299 NLS-actin expression (Fig. 6h). Of note, although this subset of ERK target genes was originally
300 defined following pulsatile ERK activation, it is likely that their expression reflects other states of
301 subtle ERK signaling as well. Nonetheless, NLS-actin expression dampens ERK activity and
302 reduces the expression of a small subset of ERK target genes, including several immediate
303 early genes that are known to inhibit pluripotency [72].
304
305 **Actin fails to accumulate in the nucleus below a threshold nuclear height**
306 The increase in reprogramming efficiency by NLS-actin was less profound than chemical ERK
307 tuning, suggesting unknown processes counteracting the cells' tuning ability even in the
308 presence of NLS-actin expression. The manipulations that changed reprogramming efficiency in
309 our experiments had consistent effects on colony morphology: colonies failing to activate
310 Oct4:GFP appeared more spread or flat. We therefore assessed if/how cell height is altered, a
311 morphologic parameter that was recently recognized to dictate cell behavior [73,74,75]. Following
312 the measurements determined in these studies, we first reprogrammed cells using a cell height
313 confiner (Fig. 7a,b) at 5 or 10 μm. While some Oct4:GFP+ colonies could be found under 10 μm
314 confinement, no Oct4:GFP+ colonies were present under 5 μm confinement (Fig. S7a). The
315 cells outside of the confinement area remained Oct4:GFP+ and had typical dome morphology,
316 indicating that the loss of Oct4:GFP is specific to the cells under height-confinement (Fig. 7b,
317 Fig. S7a). As the colonies under 10 μm confinement appeared partially flattened, we increased
318 confinement height to 20 μm. Under 20 μm, Oct4:GFP+ colonies of normal morphology
319 appeared (Fig. 7c,d, Fig. S7b). 10 μm confinement reduced the number and intensity of
320 Oct4:GFP+ cells. Under 5 μm confinement, only fibroblastic-like cells could be identified and
321 none were Oct4:GFP+. These results demonstrate that cells need to reach a minimal height of
322 10 μm to reactive *Oct4*, whereas 20 μm is the permissive cell height. Importantly, at 10 μm or 5
323 μm height, NLS-actin was no longer found inside the nucleus, indicating that sufficient cell
324 height is required for actin to enrich inside the nucleus (Fig. 7e,f). Lastly, we confined ESC
325 derived from the inner cell mass of Oct4:GFP mouse for 16 hours (Fig. 7g,h, Fig. S7c). Similar
326 to the reprogramming cells, these already pluripotent stem cells retained normal colony
327 morphology and remained Oct4:GFP+ under 20 μm confinement. 10 μm confinement partially
328 flattened the colonies and reduced Oct4:GFP intensity. Strikingly, colonies under 5 μm

confinement lost Oct4:GFP fluorescence without any other differentiation-inducing signals (Fig. 7g,h, Fig. S7c). These results indicate that cell height could alter actin's nuclear allocation, and has a dominating effect to inhibit pluripotency gene expression.

Fibroblast reprogramming cultures (e.g. day 6-8) primarily contain two types of cells readily distinguishable by morphology and/or their relationship with neighboring cells: clusters of cells appearing as colonies and those retaining fibroblast morphology (Fig. 7i, Movie S4). We determined the fibroblastic cells to have a typical nuclear height of ~5 μm, while the cells in colonies reach ~10 μm in height (Fig. 7j,k). Cells expressing NLS-actin, but not those expressing WT β-actin, or point mutants NLS-actin^{G13R} and NLS-actin^{S14C}, had nuclear height to be around or above 10 μm. Furthermore, TFII-IΔ KD or NLS-actin expression individually increased nuclear height, but their combination resulted in low nuclear height (Fig. 7l-n). Taken together, the ERK-tuning by TFII-IΔ likely mediates the actin reallocation and cell morphologic changes accompanying reprogramming.

Discussion

Yamanaka reprogramming from most somatic states is rare, which occurs stochastically, as each cell has a low, random chance of reprogramming (Fig. S6g) [76-79]. Our earlier work has revealed that reprogramming stochasticity is absent in a rare population of myeloid progenitors which exhibit unusually fast cell cycle[80,81]. Prospective isolation of the fast-cycling subpopulation of fibroblasts drastically enriches for reprogramming activity. Strikingly, these fast-cycling fibroblasts display a much less spread cell morphology [37,54,82] that we now show to being taller. One of the most profound changes that occurs during reprogramming is a switch in the biological interpretation of ERK signaling at the cellular level: in nearly all differentiated types, ERK activity is pro-proliferative, but in pluripotent stem cells ERK activity must be kept low to avoid differentiation. Fine-tuning this ERK activity transition dramatically increases reprogramming efficiency, so that most cells in culture can activate pluripotent gene expression. We propose that cell morphology integrates into cell identity regulation by titrating ERK activity: much more actin is being allocated into the nucleus as cells change identity. At least one consequence of the nuclear accumulated actin is to sequester TFII-IΔ, thereby inhibiting this mode of ERK activation. This model deepens the connection between cell morphology/mechanics and cell identity/behavior found in other biological systems [83-85], as well as in pluripotent stem cells [68,86,87].

Nuclear actin is known to be present in large quantity in frog oocyte germinal vesicles [88]. These exceptionally large cells collapse to gravity when this nuclear actin meshwork is disrupted [89]. Given this insight, it is perhaps not surprising why polymerized actin is required in the germinal vesicle to reprogram the transplanted somatic nuclei, as shown by Gurdon and colleagues [41]. Mammalian somatic cells are five orders of magnitude smaller, where the possibility that nuclear actin primarily functions by mechanical support becomes slim. However, injected somatic nuclei do undergo prominent "swelling" in this system [90]. Filamentous actin also form in mammalian somatic nucleus immediately after mitosis, expanding the compact postmitotic nucleus to that of G1 conformation; interfering with nuclear actin pool size or polymerization leads to significantly reduced nuclear volume [46]. Across these diverse biological contexts, a coherent theme appears to be nuclear actin's role in modulating the size and/or morphology of the nucleus. In this regard, we found that allocating more actin into the nucleus increases nuclear height, and sufficient height is necessary for actin's nuclear enrichment (Fig. 7).

The importance of nuclear height has only begun to be appreciated [73,74,75]. In 2D cultured cells, confining cell height to 5 μm, but not 10 μm, triggers actomyosin contractility due to stretching of the nuclear membrane and activating the mechanosensitive calcium channels leading to Ca2+ directed actomyosin contractility [73]. Similar findings are seen in cells in 3D tissues [75]. Insights from these complementary contexts paint a model for how restrictive nuclear dimensions control cell's contractility, perhaps enabling it to "run away" when severely confined. This intuitive model lends insights into why NLS-actin fail to concentrate in the flattened nucleus (Fig. 7e,f), as a contractile cytoplasm likely draws monomeric actin away from the nucleus. However, the full picture is likely more complex (e.g. whether there is involvement of nuclear Ca2+ [91] was not considered). Experimental approaches with sufficient temporal and spatial resolution/precision allowing the detection of rapid and subcellular signaling dynamics are required to further delve into this problem.

Our approach in identifying TFII-I as an actin-binding protein is inherently biased toward highly abundant nuclear proteins and/or strong binding affinity (Fig. 3a-c), suggesting potential generalizability. In mice, *Gtf2i* inactivation results in early embryonic lethality [92] . In humans, hemizygous deletion of *GTF2I* genomic region is associated with neurodevelopmental deficits known as Williams-Beuren Syndrome, while its duplication leads to autism spectrum disorders [92-94]. Single nucleotide polymorphisms at *GTF2I* loci are associated with autoimmune diseases [95-97]. A point mutation (L424H) is prevalent in thymic epithelial tumors [98]. Contrasting its importance in development and diseases, the understanding of how *GTF2I* abnormality causes diseases is limited. Our work is partly based on the previous reports on how Gtf2i/TFII-I participates in regulation via interactions with ERK [32,99,28]. The involvement for this actin-TFII-IΔ-ERK axis in other cellular contexts awaits further examination. With multiple MEK/ERK inhibitors in the clinics, our model suggestions that dosages of such pharmacologic agents need to be taken into consideration to achieve desired effects. The small subset of down-regulated genes by NLS-actin, such as *c-fos*, are well validated targets of ERK and TFII-I. How TFII-I-ERK functions to transcriptionally regulate pluripotency also awaits further investigation.

Material and Methods

Cell culture and reprogramming

All mouse work was approved by the Institutional Animal Care and Use Committee of Yale University. The reprogrammable mice with reporter (R26rtTA;Col1a14F2A;Oct4GFP) were derived by crossing reprogrammable mice with Oct4:GFP mice, which has been described before.

DNA constructs

All Actin constructs were cloned into pMSCV-IRES-blasticidin backbone. The shRNAs targeting to Xpo6, Gtf2i and its β isoform were generated by inserting the short hairpin sequence into the lentiviral backbone psi-LVRU6MP (GeneCopia), the sequences are listed in Supplementary Table 5, The pSFG-GFP, pSFG-TFII-I-GFP delta and pSFG-TFII-I-GFP Y248&249F were obtained from Addgene(#22199, #22190, #22196).

Western blotting and immunofluorescence

All procedures and antibodies used in protein analyses are listed in the accompanying supplementary materials.

RNAseq and analysis (GSEA, CellNet)

RNA-seq libraries were prepared with TruSeq Stranded mRNA Library Prep Kit (Illumina, RS-122-2101) following the manufacturer's instructions. Sequencing was performed with the Illumina HiSeq 4000 Sequencing System. For data analysis, the RNA-seq reads were mapped to mouse genome (mm10) with TopHat2 software. Gene abundance was calculated using cuffnorm, which gene expression levels and Fragments per kilobase per million (FPKM). Genes with FPKM ≥1 in two or more samples were selected for further analysis. Differentially expressed genes (DEGs) were identified by Cuffdiff followed by cutting off with FDR-adjusted P value <0.05 and fold change >2. MA plot of differentially expressed genes was also done with the R software. RNA-seq raw data and processed data have been deposited as GSE229191. GO analysis of differentially expressed genes was performed with R.

Cell height confinement

Cells were seeded and cultured in 6-well static cell confiner device (4Dcell, France) at day 6, allowed to reprogram until day 14 or 12. ImageExpress Micro 4 Imaging system were used for imaging the phase and Oct4:GFP colony counting. Leica Stellaris confocal microscope platform were used for imaging the live cell mCherry and Oct4:GFP, Oct4:GFP cell counting and measure Oct4:GFP intensity. NLS-Actin transduced cell on reprogramming day12 were fixed and stained using FLAG antibody. N/C ratio of FLAG intensity was calculated using LAS AF software. Oct4:GFP expressed ESC were seeded in 6-well static cell confiner device for 16 hours for imaging the live cells of Oct4:GFP and intensity measurement.

Construction of custom sgRNA library and screening

The online web tool CHOPCHOP (https://chopchop.cbu.uib.no/) was used to generate sgRNA designs against target genes. For each gene, 4 sgRNAs were chosen based on the location and score. Screening is done by following the Zhang Lab's protocols with minor modification.

Supplemental Materials (with full description of materials and procedures)

Four supplementary tables (Table S1-4) and movies (Movie S1-4) accompany this manuscript. Supplementary Table S5 contains sequences for all primers used.

References

1 Ware, CB. Concise Review: Lessons from Naive Human Pluripotent Cells. *Stem Cells 2017* **35**, 35.

2 Robinton, DA & Daley, GQ. The promise of induced pluripotent stem cells in research and therapy. *Nature 2012* **481**, 295.

3 Barooji, YF, Hvid, KG, Petitjean, II, Brickman, JM, Oddershede, LB & Bendix, PM. Changes in Cell Morphology and Actin Organization in Embryonic Stem Cells Cultured under Different Conditions. *Cells 2021* **10**.

4 Khatau, SB, Hale, CM, Stewart-Hutchinson, PJ, Patel, MS, Stewart, CL, Searson, PC *et al.* A perinuclear actin cap regulates nuclear shape. *Proc Natl Acad Sci U S A 2009* **106**, 19017.

5 Davidson, PM & Cadot, B. Actin on and around the Nucleus. *Trends Cell Biol 2021* **31**, 211.

6 Nag, S, Larsson, M, Robinson, RC & Burtnick, LD. Gelsolin: the tail of a molecular gymnast. *Cytoskeleton (Hoboken) 2013* **70**, 360.

475 7 Amann, KJ & Pollard, TD. The Arp2/3 complex nucleates actin filament branches from
476 the sides of pre-existing filaments. *Nat Cell Biol 2001* **3**, 306.
477 8 McGough, AM, Staiger, CJ, Min, JK & Simonetti, KD. The gelsolin family of actin
478 regulatory proteins: modular structures, versatile functions. *FEBS Lett 2003* **552**, 75.
479 9 Carley, E, King, MC & Guo, S. Integrating mechanical signals into cellular identity. *Trends*
480 *Cell Biol 2022*.
481 10 Zimmermann, D & Kovar, DR. Feeling the force: formin's role in mechanotransduction.
482 *Curr Opin Cell Biol 2019* **56**, 130.
483 11 Schwarz, US & Gardel, ML. United we stand: integrating the actin cytoskeleton and cell-
484 matrix adhesions in cellular mechanotransduction. *J Cell Sci 2012* **125**, 3051.
485 12 Papalazarou, V & Machesky, LM. The cell pushes back: The Arp2/3 complex is a key
486 orchestrator of cellular responses to environmental forces. *Curr Opin Cell Biol 2020* **68**,
487 37.
488 13 Wickstrom, SA & Roca-Cusachs, P. Special issue on "mechanotransduction in cell fate
489 determination" - From molecular switches to organ-level regulation. *Exp Cell Res 2019*
490 **382**, 111452.
491 14 Pollard, TD. Actin and Actin-Binding Proteins. *Cold Spring Harb Perspect Biol 2016* **8**.
492 15 Dominguez, R & Holmes, KC. Actin structure and function. *Annu Rev Biophys 2011* **40**,
493 169.
494 16 Plessner, M, Melak, M, Chinchilla, P, Baarlink, C & Grosse, R. Nuclear F-actin formation
495 and reorganization upon cell spreading. *J Biol Chem 2015* **290**, 11209.
496 17 Percipalle, P & Vartiainen, M. Cytoskeletal proteins in the cell nucleus: a special nuclear
497 actin perspective. *Mol Biol Cell 2019* **30**, 1781.
498 18 Plessner, M & Grosse, R. Dynamizing nuclear actin filaments. *Curr Opin Cell Biol 2019*
499 **56**, 1.
500 19 Kelpsch, DJ & Tootle, TL. Nuclear Actin: From Discovery to Function. *Anat Rec (Hoboken)*
501 *2018* **301**, 1999.
502 20 Miyamoto, K & Gurdon, JB. Nuclear actin and transcriptional activation. *Commun Integr*
503 *Biol 2011* **4**, 582.
504 21 Serebryannyy, LA, Parilla, M, Annibale, P, Cruz, CM, Laster, K, Gratton, E *et al.* Persistent
505 nuclear actin filaments inhibit transcription by RNA polymerase II. *J Cell Sci 2016* **129**,
506 3412.
507 22 Vartiainen, MK, Guettler, S, Larijani, B & Treisman, R. Nuclear actin regulates dynamic
508 subcellular localization and activity of the SRF cofactor MAL. *Science 2007* **316**, 1749.
509 23 Fiore, A, Spencer, VA, Mori, H, Carvalho, HF, Bissell, MJ & Bruni-Cardoso, A. Laminin-111
510 and the Level of Nuclear Actin Regulate Epithelial Quiescence via Exportin-6. *Cell Rep*
511 *2017* **19**, 2102.
512 24 Serebryannyy, L & de Lanerolle, P. Nuclear actin: The new normal. *Mutat Res 2020* **821**,
513 111714.
514 25 Kapoor, P, Chen, M, Winkler, DD, Luger, K & Shen, X. Evidence for monomeric actin
515 function in INO80 chromatin remodeling. *Nat Struct Mol Biol 2013* **20**, 426.
516 26 Hyrskyluoto, A & Vartiainen, MK. Regulation of nuclear actin dynamics in development
517 and disease. *Curr Opin Cell Biol 2020* **64**, 18.

518 27 Makeyev, AV & Bayarsaihan, D. Alternative splicing and promoter use in TFII-I genes.
519 *Gene 2009* **433**, 16.
520 28 Caraveo, G, van Rossum, DB, Patterson, RL, Snyder, SH & Desiderio, S. Action of TFII-I
521 outside the nucleus as an inhibitor of agonist-induced calcium entry. *Science 2006* **314**,
522 122.
523 29 Kim, DW, Cheriyath, V, Roy, AL & Cochran, BH. TFII-I enhances activation of the c-fos
524 promoter through interactions with upstream elements. *Mol Cell Biol 1998* **18**, 3310.
525 30 Kim, DW & Cochran, BH. JAK2 activates TFII-I and regulates its interaction with
526 extracellular signal-regulated kinase. *Mol Cell Biol 2001* **21**, 3387.
527 31 Cheriyath, V & Roy, AL. Alternatively spliced isoforms of TFII-I. Complex formation,
528 nuclear translocation, and differential gene regulation. *J Biol Chem 2000* **275**, 26300.
529 32 Mammoto, A, Connor, KM, Mammoto, T, Yung, CW, Huh, D, Aderman, CM *et al.* A
530 mechanosensitive transcriptional mechanism that controls angiogenesis. *Nature 2009*
531 **457**, 1103.
532 33 Hakre, S, Tussie-Luna, MI, Ashworth, T, Novina, CD, Settleman, J, Sharp, PA *et al.*
533 Opposing functions of TFII-I spliced isoforms in growth factor-induced gene expression.
534 *Mol Cell 2006* **24**, 301.
535 34 Miano, JM, Long, X & Fujiwara, K. Serum response factor: master regulator of the actin
536 cytoskeleton and contractile apparatus. *American journal of physiology. Cell physiology*
537 *2007* **292**, C70.
538 35 Miralles, F, Posern, G, Zaromytidou, AI & Treisman, R. Actin dynamics control SRF
539 activity by regulation of its coactivator MAL. *Cell 2003* **113**, 329.
540 36 Sotiropoulos, A, Gineitis, D, Copeland, J & Treisman, R. Signal-regulated activation of
541 serum response factor is mediated by changes in actin dynamics. *Cell 1999* **98**, 159.
542 37 Hu, X, Wu, Q, Zhang, J, Kim, J, Chen, X, Hartman, AA *et al.* Reprogramming progressive
543 cells display low CAG promoter activity. *Stem Cells 2021* **39**, 43.
544 38 Stadtfeld, M, Maherali, N, Borkent, M & Hochedlinger, K. A reprogrammable mouse
545 strain from gene-targeted embryonic stem cells. *Nat Methods 2010* **7**, 53.
546 39 Hochedlinger, K, Yamada, Y, Beard, C & Jaenisch, R. Ectopic expression of Oct-4 blocks
547 progenitor-cell differentiation and causes dysplasia in epithelial tissues. *Cell 2005* **121**,
548 465.
549 40 Posern, G, Sotiropoulos, A & Treisman, R. Mutant actins demonstrate a role for
550 unpolymerized actin in control of transcription by serum response factor. *Mol Biol Cell*
551 *2002* **13**, 4167.
552 41 Miyamoto, K, Pasque, V, Jullien, J & Gurdon, JB. Nuclear actin polymerization is required
553 for transcriptional reprogramming of Oct4 by oocytes. *Genes Dev 2011* **25**, 946.
554 42 Esnault, C, Stewart, A, Gualdrini, F, East, P, Horswell, S, Matthews, N *et al.* Rho-actin
555 signaling to the MRTF coactivators dominates the immediate transcriptional response to
556 serum in fibroblasts. *Genes Dev 2014* **28**, 943.
557 43 Subramanian, A, Tamayo, P, Mootha, VK, Mukherjee, S, Ebert, BL, Gillette, MA *et al.*
558 Gene set enrichment analysis: a knowledge-based approach for interpreting genome-
559 wide expression profiles. *Proc Natl Acad Sci U S A 2005* **102**, 15545.
560 44 Polo, JM, Anderssen, E, Walsh, RM, Schwarz, BA, Nefzger, CM, Lim, SM *et al.* A
561 molecular roadmap of reprogramming somatic cells into iPS cells. *Cell 2012* **151**, 1617.

562 45 Schrank, BR, Aparicio, T, Li, Y, Chang, W, Chait, BT, Gundersen, GG *et al.* Nuclear ARP2/3
563 drives DNA break clustering for homology-directed repair. *Nature 2018* **559**, 61.
564 46 Baarlink, C, Plessner, M, Sherrard, A, Morita, K, Misu, S, Virant, D *et al.* A transient pool
565 of nuclear F-actin at mitotic exit controls chromatin organization. *Nat Cell Biol 2017* **19**,
566 1389.
567 47 Caridi, CP, Plessner, M, Grosse, R & Chiolo, I. Nuclear actin filaments in DNA repair
568 dynamics. *Nat Cell Biol 2019* **21**, 1068.
569 48 Caridi, CP, D'Agostino, C, Ryu, T, Zapotoczny, G, Delabaere, L, Li, X *et al.* Nuclear F-actin
570 and myosins drive relocalization of heterochromatic breaks. *Nature 2018* **559**, 54.
571 49 Dopie, J, Skarp, KP, Rajakyla, EK, Tanhuanpaa, K & Vartiainen, MK. Active maintenance
572 of nuclear actin by importin 9 supports transcription. *Proc Natl Acad Sci U S A 2012* **109**,
573 E544.
574 50 Hurst, V, Shimada, K & Gasser, SM. Nuclear Actin and Actin-Binding Proteins in DNA
575 Repair. *Trends Cell Biol 2019* **29**, 462.
576 51 Spencer, VA, Costes, S, Inman, JL, Xu, R, Chen, J, Hendzel, MJ *et al.* Depletion of nuclear
577 actin is a key mediator of quiescence in epithelial cells. *J Cell Sci 2011* **124**, 123.
578 52 Parisis, N, Krasinska, L, Harker, B, Urbach, S, Rossignol, M, Camasses, A *et al.* Initiation of
579 DNA replication requires actin dynamics and formin activity. *EMBO J 2017* **36**, 3212.
580 53 Nieminuszczy, J, Martin, PR, Broderick, R, Krwawicz, J, Kanellou, A, Mocanu, C *et al.*
581 Actin nucleators safeguard replication forks by limiting nascent strand degradation.
582 *Nucleic Acids Res 2023*.
583 54 Hartman, AA, Scalf, SM, Zhang, J, Hu, X, Chen, X, Eastman, AE *et al.* YAP Non-cell-
584 autonomously Promotes Pluripotency Induction in Mouse Cells. *Stem Cell Reports 2020*
585 **14**, 730.
586 55 Morris, SA, Cahan, P, Li, H, Zhao, AM, San Roman, AK, Shivdasani, RA *et al.* Dissecting
587 engineered cell types and enhancing cell fate conversion via CellNet. *Cell 2014* **158**, 889.
588 56 Wang, B, Wang, M, Zhang, W, Xiao, T, Chen, CH, Wu, A *et al.* Integrative analysis of
589 pooled CRISPR genetic screens using MAGeCKFlute. *Nat Protoc 2019* **14**, 756.
590 57 Li, W, Xu, H, Xiao, T, Cong, L, Love, MI, Zhang, F *et al.* MAGeCK enables robust
591 identification of essential genes from genome-scale CRISPR/Cas9 knockout screens.
592 *Genome Biol 2014* **15**, 554.
593 58 Yang, CS, Chang, KY & Rana, TM. Genome-wide functional analysis reveals factors
594 needed at the transition steps of induced reprogramming. *Cell Rep 2014* **8**, 327.
595 59 Roy, AL, Du, H, Gregor, PD, Novina, CD, Martinez, E & Roeder, RG. Cloning of an inr-and
596 E-box-binding protein, TFII-I, that interacts physically and functionally with USF1. *The*
597 *EMBO journal 1997* **16**, 7091.
598 60 Roy, AL. Pathophysiology of TFII-I: Old Guard Wearing New Hats. *Trends Mol Med 2017*
599 **23**, 501.
600 61 Hamilton, WB & Brickman, JM. Erk signaling suppresses embryonic stem cell self-
601 renewal to specify endoderm. *Cell Rep 2014* **9**, 2056.
602 62 Kim, SH, Kim, MO, Cho, YY, Yao, K, Kim, DJ, Jeong, CH *et al.* ERK1 phosphorylates Nanog
603 to regulate protein stability and stem cell self-renewal. *Stem Cell Res 2014* **13**, 1.

604 63 Chen, H, Guo, R, Zhang, Q, Guo, H, Yang, M, Wu, Z *et al.* Erk signaling is indispensable for
605 genomic stability and self-renewal of mouse embryonic stem cells. *Proc Natl Acad Sci U*
606 *S A 2015* **112**, E5936.
607 64 Ma, X, Chen, H & Chen, L. A dual role of Erk signaling in embryonic stem cells. *Exp*
608 *Hematol 2016* **44**, 151.
609 65 Ying, QL, Wray, J, Nichols, J, Batlle-Morera, L, Doble, B, Woodgett, J *et al.* The ground
610 state of embryonic stem cell self-renewal. *Nature 2008* **453**, 519.
611 66 Simon, CS, Rahman, S, Raina, D, Schroter, C & Hadjantonakis, AK. Live Visualization of
612 ERK Activity in the Mouse Blastocyst Reveals Lineage-Specific Signaling Dynamics. *Dev*
613 *Cell 2020* **55**, 341.
614 67 Hamilton, WB, Mosesson, Y, Monteiro, RS, Emdal, KB, Knudsen, TE, Francavilla, C *et al.*
615 Dynamic lineage priming is driven via direct enhancer regulation by ERK. *Nature 2019*
616 **575**, 355.
617 68 De Belly, H, Stubb, A, Yanagida, A, Labouesse, C, Jones, PH, Paluch, EK *et al.* Membrane
618 Tension Gates ERK-Mediated Regulation of Pluripotent Cell Fate. *Cell Stem Cell 2021* **28**,
619 273.
620 69 Regot, S, Hughey, JJ, Bajar, BT, Carrasco, S & Covert, MW. High-sensitivity
621 measurements of multiple kinase activities in live single cells. *Cell 2014* **157**, 1724.
622 70 de la Cova, C, Townley, R, Regot, S & Greenwald, I. A Real-Time Biosensor for ERK
623 Activity Reveals Signaling Dynamics during C. elegans Cell Fate Specification. *Dev Cell*
624 *2017* **42**, 542.
625 71 Aoki, K, Kumagai, Y, Sakurai, A, Komatsu, N, Fujita, Y, Shionyu, C *et al.* Stochastic ERK
626 activation induced by noise and cell-to-cell propagation regulates cell density-
627 dependent proliferation. *Mol Cell 2013* **52**, 529.
628 72 Liu, J, Han, Q, Peng, T, Peng, M, Wei, B, Li, D *et al.* The oncogene c-Jun impedes somatic
629 cell reprogramming. *Nat Cell Biol 2015* **17**, 856.
630 73 Lomakin, AJ, Cattin, CJ, Cuvelier, D, Alraies, Z, Molina, M, Nader, GPF *et al.* The nucleus
631 acts as a ruler tailoring cell responses to spatial constraints. *Science 2020* **370**.
632 74 Shen, Z & Niethammer, P. A cellular sense of space and pressure. *Science 2020* **370**,
633 295.
634 75 Venturini, V, Pezzano, F, Catala Castro, F, Hakkinen, HM, Jimenez-Delgado, S, Colomer-
635 Rosell, M *et al.* The nucleus measures shape changes for cellular proprioception to
636 control dynamic cell behavior. *Science 2020* **370**.
637 76 Yamanaka, S. Elite and stochastic models for induced pluripotent stem cell generation.
638 *Nature 2009* **460**, 49.
639 77 Hanna, J, Saha, K, Pando, B, van Zon, J, Lengner, CJ, Creyghton, MP *et al.* Direct cell
640 reprogramming is a stochastic process amenable to acceleration. *Nature 2009* **462**, 595.
641 78 Buganim, Y, Faddah, DA, Cheng, AW, Itskovich, E, Markoulaki, S, Ganz, K *et al.* Single-cell
642 expression analyses during cellular reprogramming reveal an early stochastic and a late
643 hierarchic phase. *Cell 2012* **150**, 1209.
644 79 Liu, LL, Brumbaugh, J, Bar-Nur, O, Smith, Z, Stadtfeld, M, Meissner, A *et al.* Probabilistic
645 Modeling of Reprogramming to Induced Pluripotent Stem Cells. *Cell Rep 2016* **17**, 3395.
646 80 Guo, S, Zi, X, Schulz, VP, Cheng, J, Zhong, M, Koochaki, SH *et al.* Nonstochastic
647 reprogramming from a privileged somatic cell state. *Cell 2014* **156**, 649.

648 81 Megyola, CM, Gao, Y, Teixeira, AM, Cheng, J, Heydari, K, Cheng, EC *et al.* Dynamic
649 migration and cell-cell interactions of early reprogramming revealed by high-resolution
650 time-lapse imaging. *Stem Cells 2013* **31**, 895.
651 82 Hu, X, Liu, ZZ, Chen, X, Schulz, VP, Kumar, A, Hartman, AA *et al.* MKL1-actin pathway
652 restricts chromatin accessibility and prevents mature pluripotency activation. *Nat*
653 *Commun 2019* **10**, 1695.
654 83 Sailem, HZ & Bakal, C. Identification of clinically predictive metagenes that encode
655 components of a network coupling cell shape to transcription by image-omics. *Genome*
656 *Res 2017* **27**, 196.
657 84 Aoki, K, Kondo, Y, Naoki, H, Hiratsuka, T, Itoh, RE & Matsuda, M. Propagating Wave of
658 ERK Activation Orients Collective Cell Migration. *Dev Cell 2017* **43**, 305.
659 85 Farahani, PE, Lemke, SB, Dine, E, Uribe, G, Toettcher, JE & Nelson, CM. Substratum
660 stiffness regulates Erk signaling dynamics through receptor-level control. *Cell Rep 2021*
661 **37**, 110181.
662 86 Bergert, M, Lembo, S, Sharma, S, Russo, L, Milovanovic, D, Gretarsson, KH *et al.* Cell
663 Surface Mechanics Gate Embryonic Stem Cell Differentiation. *Cell Stem Cell 2021* **28**,
664 209.
665 87 Wong, SY, Soto, J & Li, S. Biophysical regulation of cell reprogramming. *Curr Opin Chem*
666 *Eng 2017* **15**, 95.
667 88 Clark, TG & Merriam, RW. Diffusible and bound actin nuclei of Xenopus laevis oocytes.
668 *Cell 1977* **12**, 883.
669 89 Feric, M & Brangwynne, CP. A nuclear F-actin scaffold stabilizes ribonucleoprotein
670 droplets against gravity in large cells. *Nat Cell Biol 2013* **15**, 1253.
671 90 Gurdon, JB. Injected nuclei in frog oocytes: fate, enlargement, and chromatin dispersal. *J*
672 *Embryol Exp Morphol 1976* **36**, 523.
673 91 Nava, MM, Miroshnikova, YA, Biggs, LC, Whitefield, DB, Metge, F, Boucas, J *et al.*
674 Heterochromatin-Driven Nuclear Softening Protects the Genome against Mechanical
675 Stress-Induced Damage. *Cell 2020* **181**, 800.
676 92 Enkhmandakh, B, Makeyev, AV, Erdenechimeg, L, Ruddle, FH, Chimge, NO, Tussie-Luna,
677 MI *et al.* Essential functions of the Williams-Beuren syndrome-associated TFII-I genes in
678 embryonic development. *Proc Natl Acad Sci U S A 2009* **106**, 181.
679 93 Chailangkarn, T, Noree, C & Muotri, AR. The contribution of GTF2I haploinsufficiency to
680 Williams syndrome. *Mol Cell Probes 2018* **40**, 45.
681 94 Mervis, CB, Dida, J, Lam, E, Crawford-Zelli, NA, Young, EJ, Henderson, DR *et al.*
682 Duplication of GTF2I results in separation anxiety in mice and humans. *Am J Hum Genet*
683 *2012* **90**, 1064.
684 95 Meng, Y, He, Y, Zhang, J, Xie, Q, Yang, M, Chen, Y *et al.* Association of GTF2I gene
685 polymorphisms with renal involvement of systemic lupus erythematosus in a Chinese
686 population. *Medicine (Baltimore) 2019* **98**, e16716.
687 96 Kim, K, Bang, SY, Ikari, K, Yoo, DH, Cho, SK, Choi, CB *et al.* Association-heterogeneity
688 mapping identifies an Asian-specific association of the GTF2I locus with rheumatoid
689 arthritis. *Sci Rep 2016* **6**, 27563.

690 97 Li, Y, Zhang, K, Chen, H, Sun, F, Xu, J, Wu, Z *et al.* A genome-wide association study in
691 Han Chinese identifies a susceptibility locus for primary Sjogren's syndrome at 7q11.23.
692 *Nat Genet 2013* **45**, 1361.
693 98 Petrini, I, Meltzer, PS, Kim, IK, Lucchi, M, Park, KS, Fontanini, G *et al.* A specific missense
694 mutation in GTF2I occurs at high frequency in thymic epithelial tumors. *Nat Genet 2014*
695 **46**, 844.
696 99 Jiang, W, Sordella, R, Chen, GC, Hakre, S, Roy, AL & Settleman, J. An FF domain-
697 dependent protein interaction mediates a signaling pathway for growth factor-induced
698 gene expression. *Mol Cell 2005* **17**, 23.
699

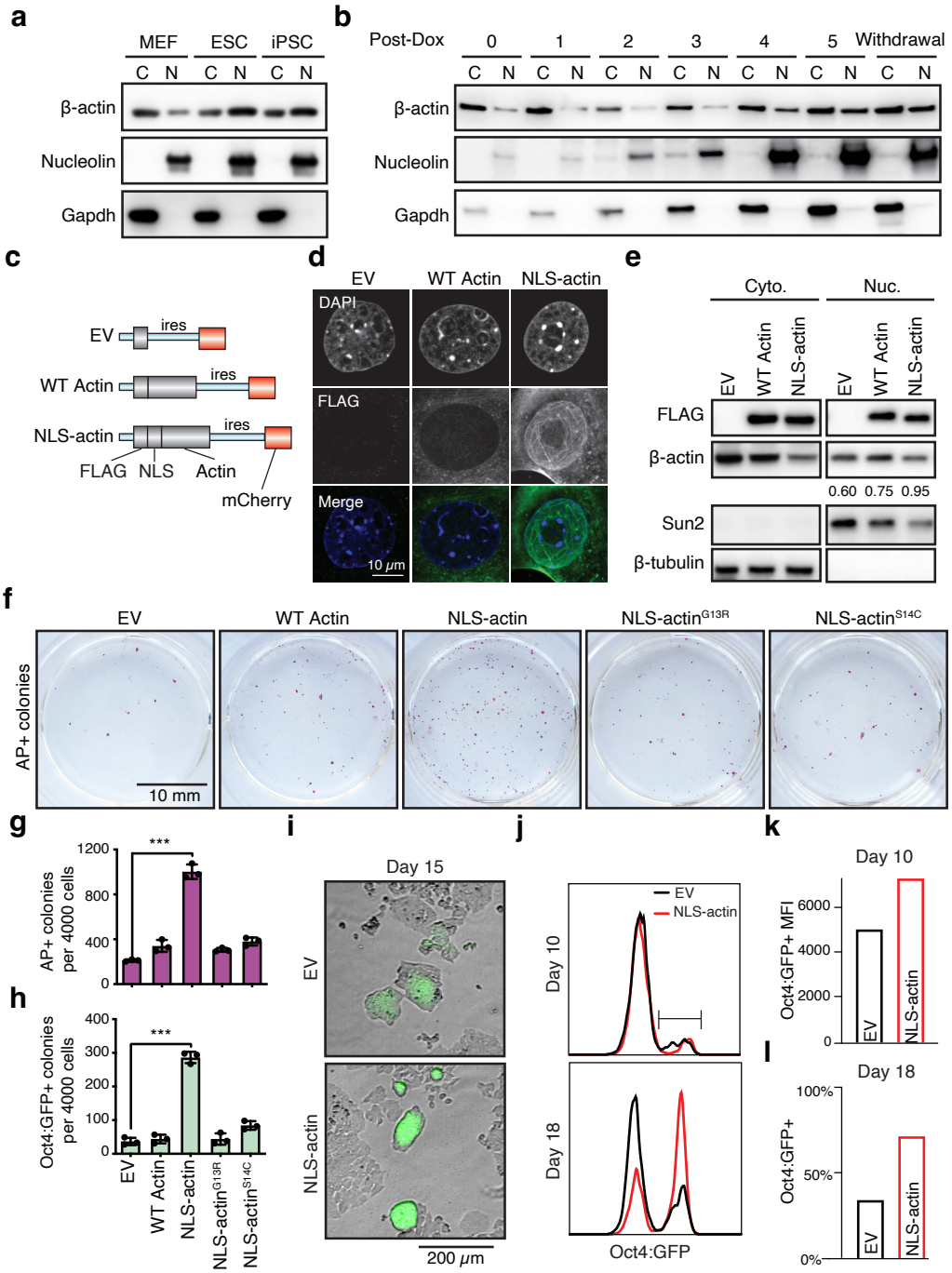

Fig. 1. More actin in the nucleus favors pluripotency. **a,b** Representative western blot analysis of the cytoplasmic (C) and nuclear (N) fraction of actin in **(a)** MEF, ESC and iPSC, and **(b)** Hematopoietic progenitors undergoing reprogramming, sampled at daily intervals for 5 days. Withdrawal denotes cells 3 days after Dox removal. Nucleolin and Gapdh control for nuclear and cytoplasmic proteins, respectively. **c** Retroviral constructs for expressing NLS-actin, WT actin and the empty vector (EV) control. **d** Immunofluorescence (IF) of FLAG in MEFs transduced with constructs shown in c. **e** Representative western blot analysis validating FLAG-tagged actin in the nuclear fraction of MEFs transduced with constructs shown in c. Sun2 and β-tubulin control for nuclear and cytoplasmic proteins, respectively. The numbers denote the ratio between nuclear and cytoplasmic actin band intensity. **f-h:** Reprogrammable MEFs transduced with various actin constructs were selected/sorted (4000 cells), and plated on feeders for reprogramming. **(f)** Representative images of Alkaline Phosphatase positive (AP+) colonies on reprogramming day 10. **(g)** Quantification of AP+ colonies, ***$P < 0.001$, n=3. **(h).** Quantification of Oct4:GFP+ colonies as in g. ***$P < 0.001$, n=3. **i-l** Reprogramming were conducted without feeders. **(i)** Representative images of bright field and Oct4:GFP overlay on day 15 **(j)** Oct4:GFP FACS histogram on day 10 and 18. **(k)** Mean fluorescence intensity (MFI) of Oct4:GFP on day 10. **(l)** %Oct4:GFP+ on day 18.

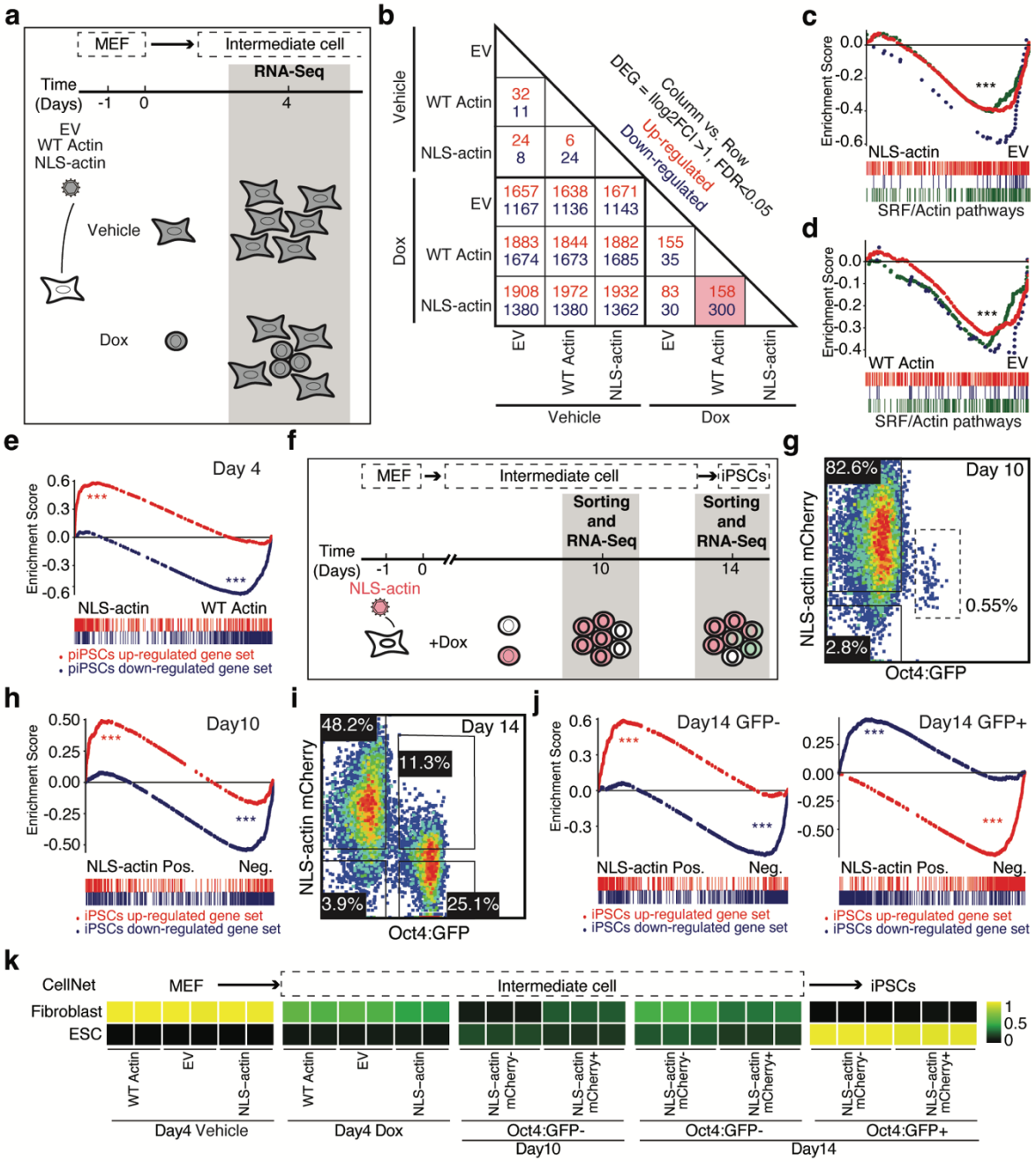

Fig. 2. NLS-actin promotes somatic cell reprogramming defying known mechanisms. a Experimental workflow for harvesting cells in RNA-seq analysis. Reprogrammable MEF transduced with EV, WT actin or NLS-actin were cultured in Vehicle or Dox for 4 days before total RNA was harvested. **b** Differentially expressed genes (DEGs) in pair-wise comparisons across all sample groups. **c, d** Gene set enrichment analysis (GSEA) detected decreased SRF target genes in **(c)** NLS-actin and **(d)** WT actin expressing cells as compared to EV. Three SRF target gene sets (green, red, blue lines) showed consistent results ***$P < 0.001$. **e** GSEA enrichment of up-(red) and down-(blue) regulated gene sets in pre-iPSC (piPSC), in day 4 NLS-actin versus WT actin expressing cells. ***$P < 0.001$. **f** Experimental scheme for comparing cells within the same culture, distinguishable by mCherry. **g** FACS plot of day 10 reprogramming cells which contain a small population (0.55%) of Oct4:GFP+ cells, with the majority being mCherry+. **h** GSEA enrichment of up-(red) and down-(blue) regulated gene sets in iPSCs, in day 10 Oct4:GFP- cells, between the NLS-actin mCherry positive (Pos.) and negative (Neg.) populations in g.***$P < 0.001$. **i** FACS plot of day 14 reprogramming cells. Four populations distinguishable by mCherry and Oct4:GFP were sorted for RNA-Seq. **j** GSEA enrichment of up-(red) and down-(blue) regulated gene sets in iPSCs, in day 14 cells between the NLS-actin mCherry positive (Pos.) and negative (Neg.) populations from Oct4:GFP- (left) and Oct4:GFP+ (right) groups in i. ***$P < 0.001$. **k** CellNet analysis of all samples over time. Bright yellow denotes high similarity and black denotes dissimilarity to reference cell types MEF and ESC.

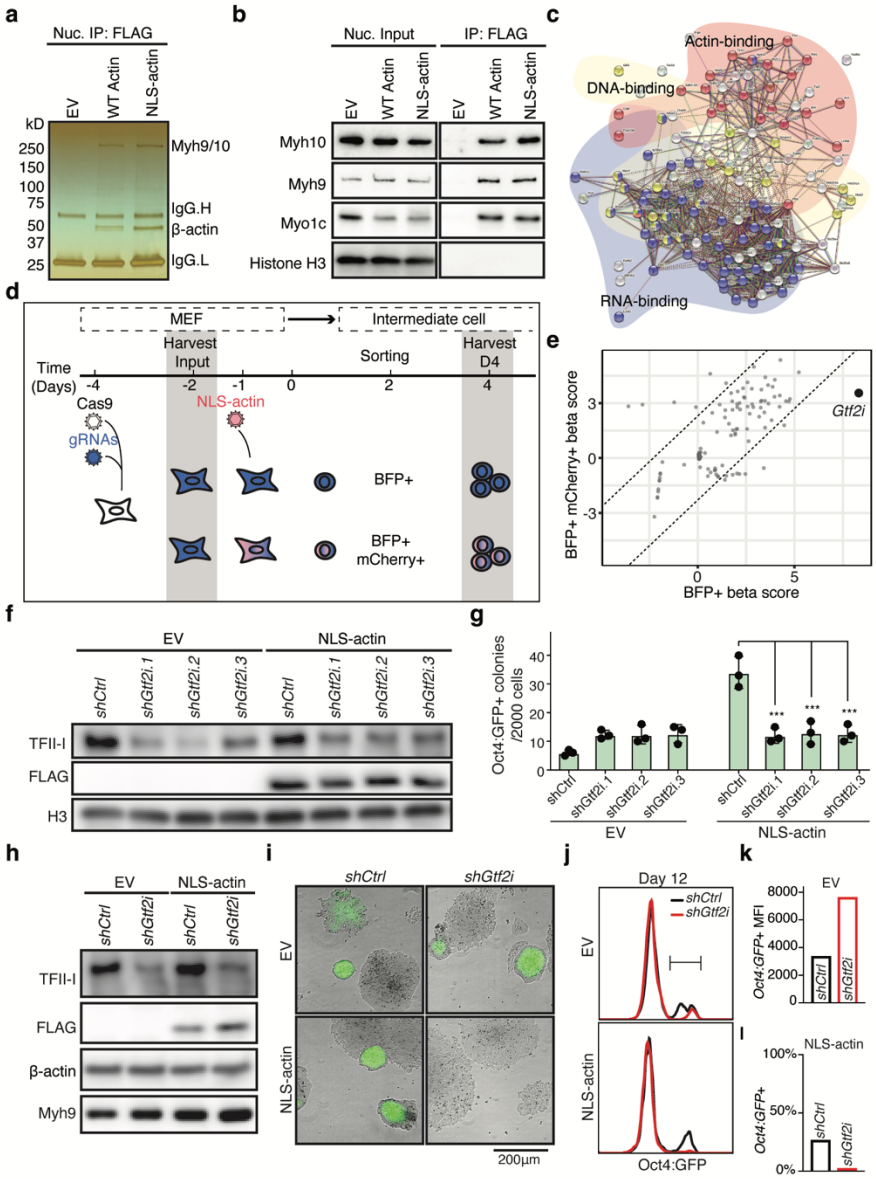

Fig. 3. *Gtf2i*/TFII-I is required for NLS-actin to promote reprogramming. a,b,c Co-immunoprecipitation followed by mass spectrometry for identifying nuclear actin interacting proteins. **(a)** SDS-PAGE and silver staining of the nuclear protein immunoprecipitants by FLAG antibody on day 6 reprogramming MEFs. **(b)** Western blot with antibodies specific for Myh9, Myh10 and Myo1c on the immunoprecipitated protein, with Histone H3 as a control. **(c)** STRING analysis of 122 candidate nuclear actin interacting proteins containing three categories: actin binding proteins (pink), DNA binding proteins (yellow) and RNA binding proteins (blue). **d,e** CRISPR screen identifying mediator(s) of nuclear actin to promote reprogramming. **(d)** Experimental scheme of the screen. Custom gRNAs library targeting the 122 candidate genes and 10 additional control genes (4 gRNAs per gene) were constructed, which also co-express Blue Fluorescence Protein (BFP). Cas9-expressing vector (also expresses blasticidin resistance) were transduced into reprogrammable MEFs and selected by blasticidin. Input DNA was collected before NLS-actin (mCherry+) transduction and Dox treatment. BFP+ cells were sorted into mCherry+/- population and continued reprogramming. On reprogramming day 4, DNA from enough BFP+ and BFP+/mCherry+ cells were collected to provide ~150x coverage. **(e)** Normalized beta score of BFP+ and BFP+mCherry+ gRNA reads against input. gRNAs targeting *Gtf2i* are depleted in BFP+mCherry+ cells. **f** Western blot analysis for TFII-I protein in MEFs transduced with EV or NLS-actin, expressing individual shRNAs targeting *Gtf2i*, using Histone H3 as a loading control. **g** Quantification of Oct4:GFP+ colonies on day 10, from cells shown in f. n=3. **h** Western blot analysis for TFII-I protein in MEFs expressing EV or NLS-actin expressing the three pooled *Gtf2i* shRNAs, with Myh9 as a loading control. **i** Representative bright field and Oct4:GFP images on day 15 from cells in h. **j** FACS histogram of Oct4:GFP on day 12. **k** Quantification of the mean fluorescence intensity (MFI) of Oct4:GFP in EV cells. **l** %Oct4:GFP+ on day 12 in NLS-actin expressing cells. MFI was not quantified in these cells due to their absence.

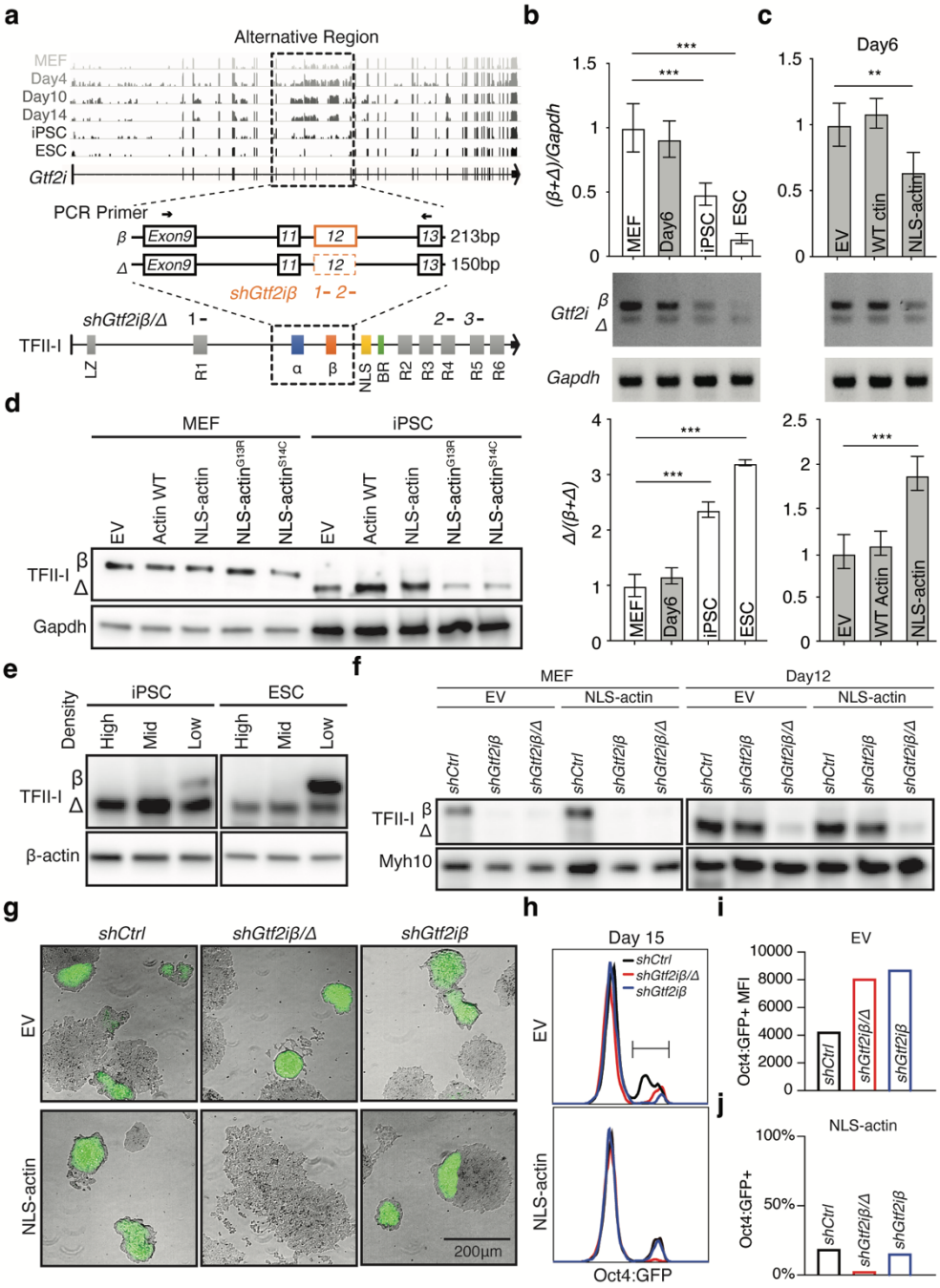

Fig. 4 The delta isoform of Gtf2i, TFII-IΔ, mediates NLS-actin's pro-reprogramming effect. a Top: RNA-seq reads during reprogramming mapping to the *Gtf2i* gene. Box depicts the region of alternative exons. Middle: Schematic of the alternative exons, highlighting the difference between β and Δ isoforms. Exon 12 (orange box) is present in β and absent in Δ. The black arrows above the exons denote positions of qPCR primers, with the anticipated PCR amplicon sizes in base pairs (bp). Bottom: Schematic of TFII-I protein isoforms. The shRNAs used in Fig. 3 are shown as three short black bars, with the β specific shRNAs shown as two orange bars. **b** RT-qPCR products using primers shown in **a** from different cell types. The PCR products contain two bands, corresponding to the β and Δ isoforms. Quantification of the total product level normalized to *Gapdh* is shown on top and the Δ/(β+Δ) ratio below. **c** Similar to b, qPCR products from reprogramming day 6 cells expressing the indicated constructs. **d** Western blot analysis of TFII-I protein in MEFs expressing the actin constructs and the iPSC derived from the respective MEFs, with Gapdh as a loading control. **e** Western blot analysis of TFII-I protein in iPSC and ESC plated at different densities. **f** Western blot for TFII-I in reprogrammable MEFs transduced with β-specific or β/Δ dual targeting shRNAs. Extracts were harvested from MEFs before reprogramming and on day 12, with Myh10 as a loading control. **g** Representative bright field and Oct4:GFP fluorescence of reprogramming cultures on day 15. **h** Oct4:GFP analysis by FACS for cells shown in g. **i** MFI of Oct4:GFP in EV cells. **j** %Oct4:GFP+ in NLS-actin expressing cells. Note the absence of Oct4:GFP+ cells with β/Δ dual targeting shRNAs.

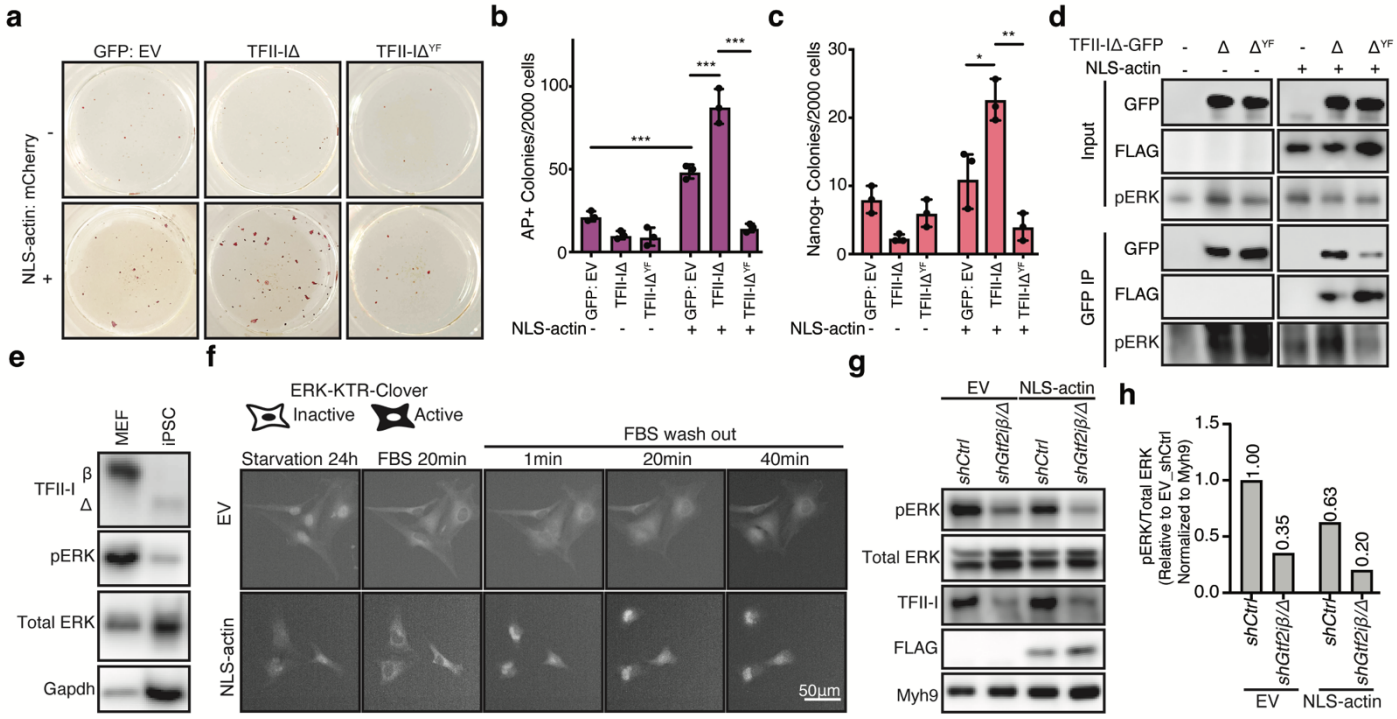

Fig. 5. Inhibiting TFII-IΔ while co-expressing NLS-actin reduces pERK to a level not permissive for reprogramming. **a** Representative AP+ colonies formed by cells overexpressing WT TFII-IΔ or the Y248F (YF) mutant on day 10. **b** Quantification of AP+ colonies shown in a. n=3. **c** Cultures shown in a were stained by Nanog specific antibody (since the TFII-IΔ constructs co-express GFP) and quantified. n=3. **d** Western blot analyses for FLAG and pERK following co-IP with GFP antibody in cells transduced with EV, WT or YF TFII-I, with or without NLS-actin co-expression. **e** Western blot for TFII-I and pERK in MEF and iPSC, with total ERK and Gapdh as controls. **f** Time-lapse images of ERK-KTR-Clover in EV or NLS-actin expressing fibroblasts, serum starved for 24 hours before stimulated for imaging. **g** Western blot for pERK levels in EV or NLS-actin expressing MEFs in the presence of β/Δ dual targeting shRNAs, with Myh9 as a loading control. **h** Quantification of pERK/ERK ratio normalized to Myh9 shown in g.

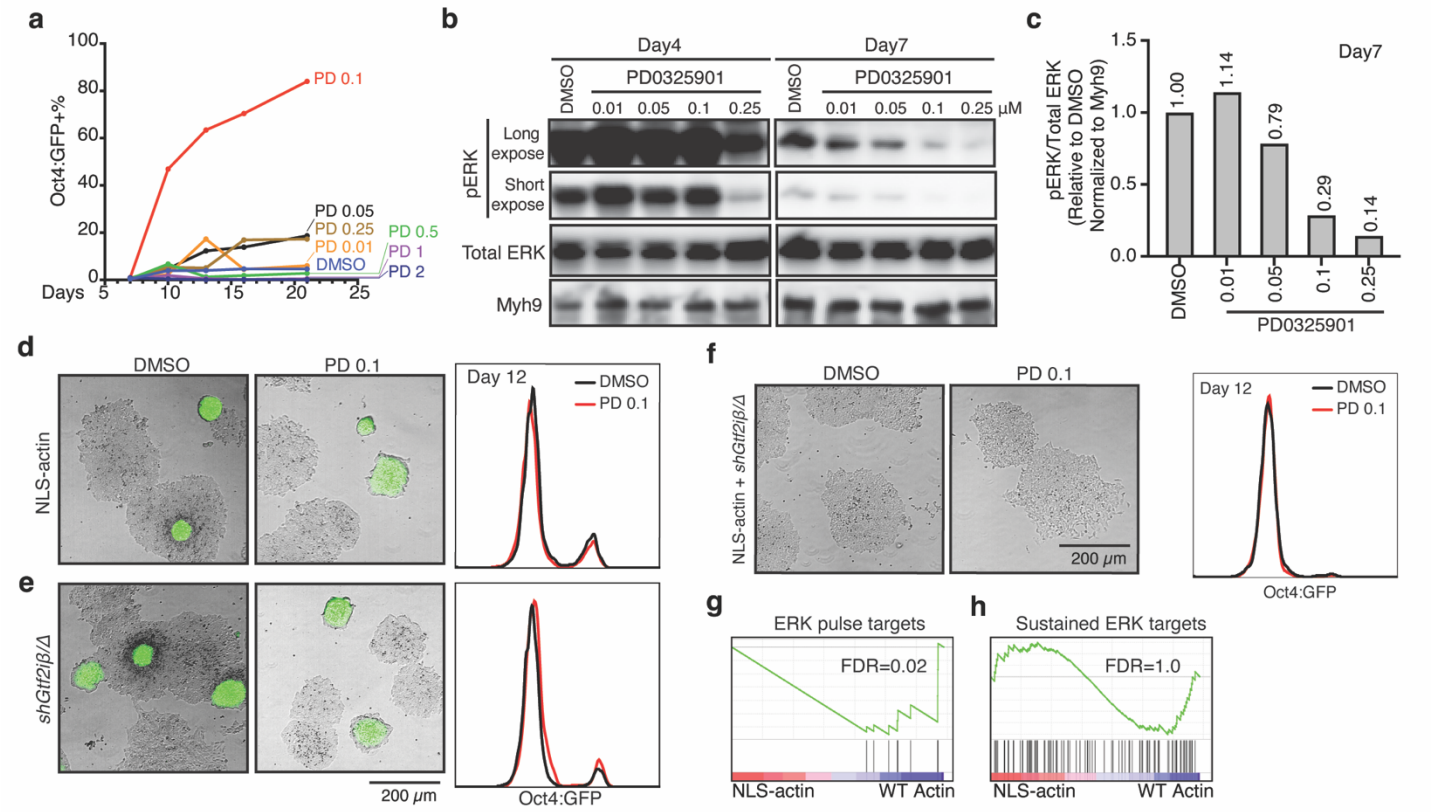

Fig. 6. Mild ERK inhibition by chemical inhibitors promotes reprogramming from most fibroblasts. a %Oct4:GFP+ cells arising in reprogramming cultures treated with different concentrations of PD0325901 over time (days), as determined by FACS. **b** Western blot analysis for pERK and total ERK in the presence of various PD0325901 concentrations, harvested on day 4 and 7. **c** Quantification of the pERK/ERK ratio, normalized to Myh9 on day 7 as shown in b. **d-f** Representative bright field and Oct4:GFP fluorescence and their corresponding FACS plots in 0.1μM PD0325901 (PD 0.1) on day 15 in cells expressing NLS-actin **(d)** or pooled β/Δ targeting shRNAs **(e)**, or both **(f). g** A subset of ERK targets, defined as the "ERK pulse targets" is downregulated by NLS-actin as compared to cells expressing WT actin in the same RNA-seq results shown in Fig. 2b. **h** Most other ERK target genes, defined as the "Sustained ERK targets" show no difference.

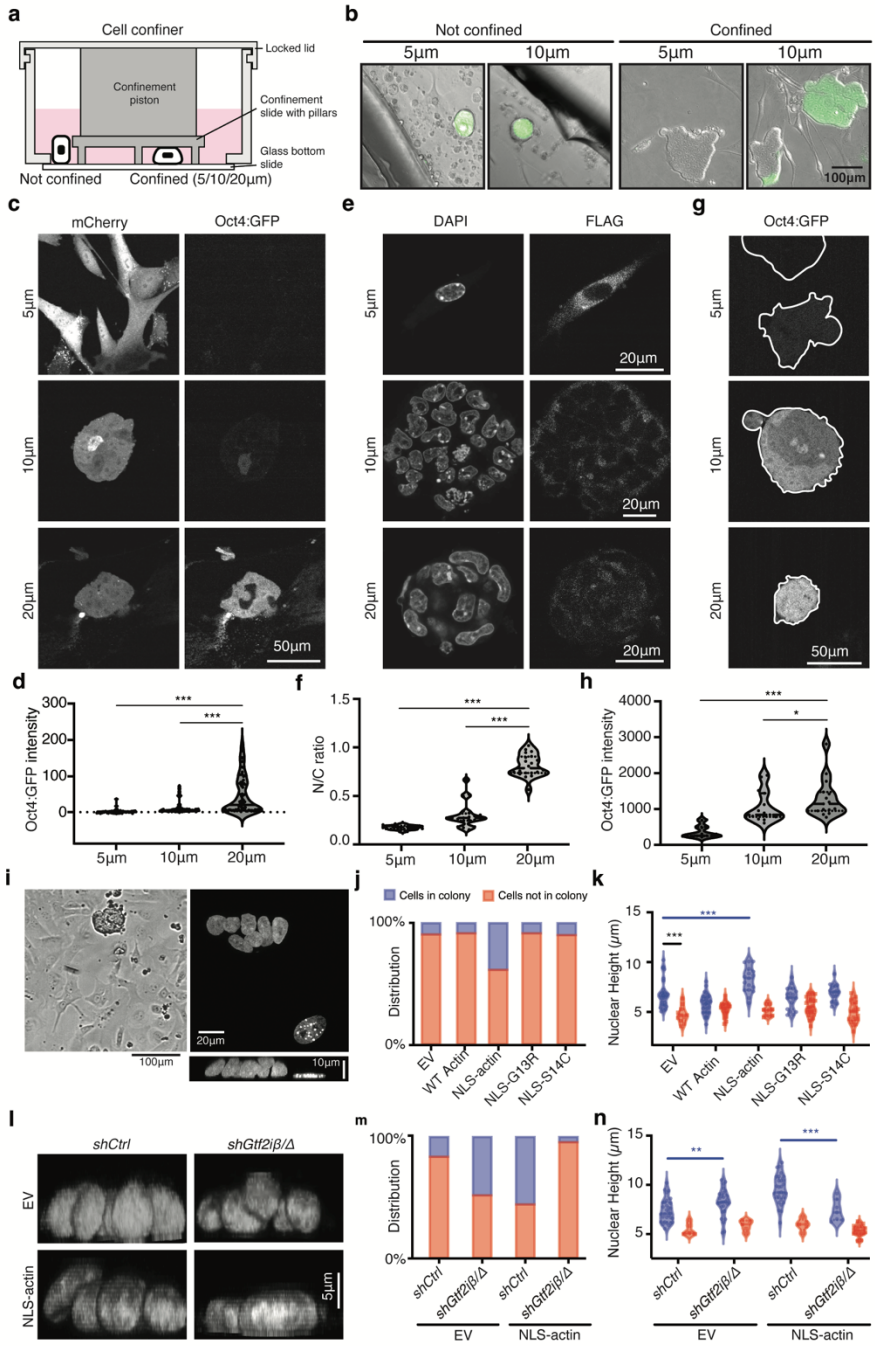

Fig. 7 Actin fails to accumulate in the nucleus below a threshold nuclear height. a Schematic of the cell height confiner, depicting height-confined cells and unconfined cells outside of the confinement area. **b** Representative bright field and Oct4:GFP fluorescence of cells and colonies under 5 or 10 µm confinement on reprogramming day 14. Cells outside of the confinement area are shown as controls. **c** NLS-actin expressing cells on day 12 under different height confinement. **d** Quantification of Oct4:GFP fluorescence intensity of cells in c, ***$p < 0.001$, n=50. **e** FLAG IF on cells similar to those in c. **f** Quantification of the nuclear:cytoplasmic (N:C) FLAG signals for cells in e, ***$p < 0.001$, n=20. **g** Oct4:GFP+ ESC under height confinement. **h** Quantification of Oct4:GFP fluorescence intensity of cells in g. Solid white line marks the boundary of colonies. n=15. *$p < 0.05$, ***$p < 0.001$. **i** Representative images showing two typical types of cells on day 6-8 of MEF reprogramming. Left (low power bright field): a small colony surrounded by fibroblast-like cells. Right (high power with side/z-view): DAPI stained cells imaged by confocal microscopy depicting a small cluster of cells and one lone cell on the side. **j** Numeric frequency of the two types of cells expressing the indicated actin constructs on day 6 of reprogramming. **k** Quantification of nuclear height of the two types of cells in j. n =11-35. ***$p < 0.001$. **l** Representative z-view of DAPI stained reprogramming culture on day 6, from cells expressing EV or NLS-actin in combination with β/Δ dual targeting shRNAs. **m** Numeric frequency of the two types of cells in l. **n** Quantification of nuclear height of the two types of cells in l. n = 5-31. **$p < 0.01$. ***$p < 0.001$.

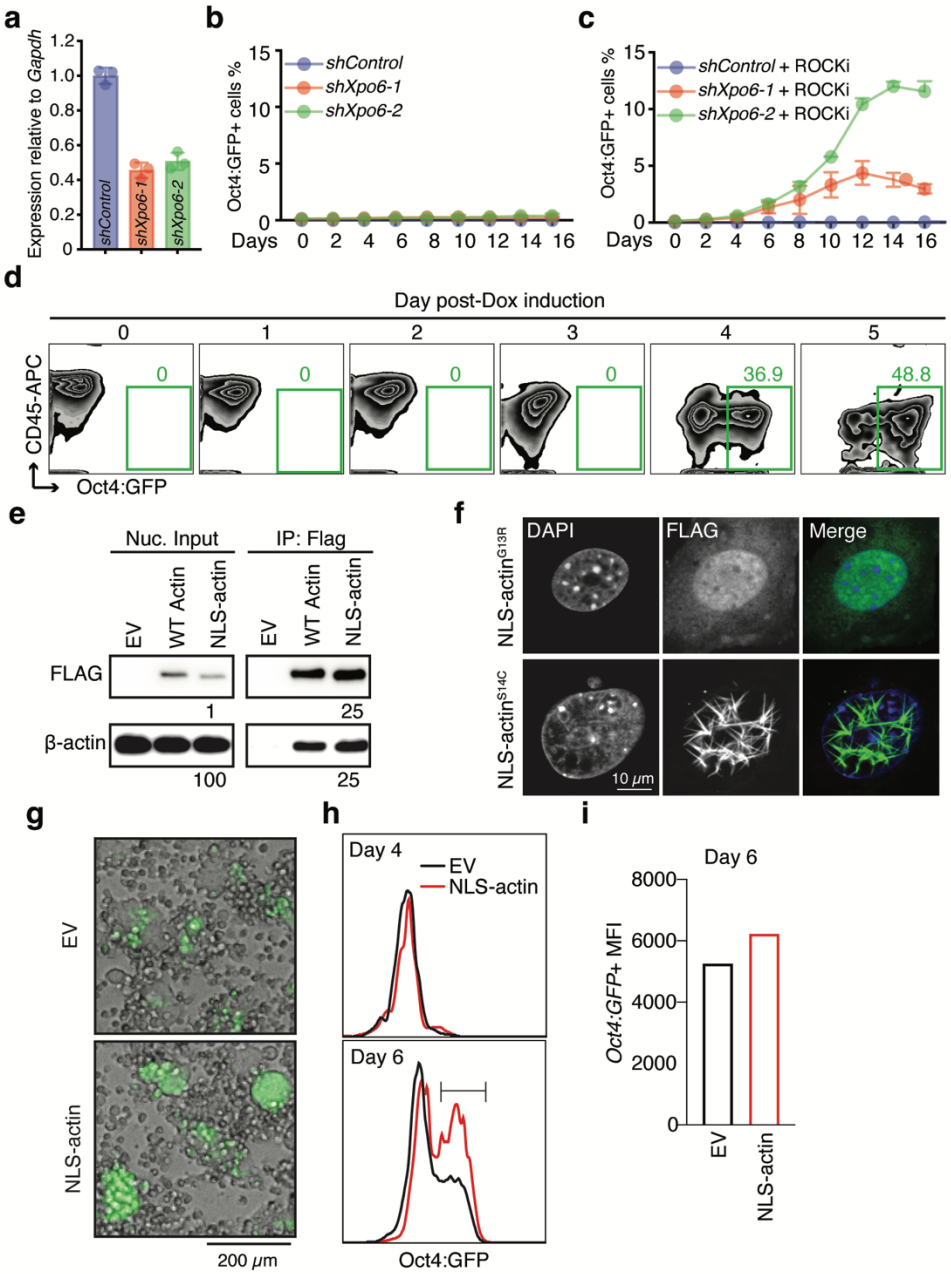

Fig. S1. More actin in the nucleus favors pluripotency. **a** Realtime RT-qPCR analysis of *Xpo6* in caMKL1-blocked cells, transduced with shRNAs targeting *Xpo6* or control shRNA (shControl), normalized to *Gapdh*. n=3. **b,c** caMKL1-blocked cells were rescued by *Xpo6* shRNAs in the absence **(b)** or presence **(c)** of ROCK inhibitor (ROCKi), as determined by the emergence of Oct4:GFP+ cells. The rescue efficiency is similar to what was reported for members of the actomyosin-LINC system. **d** Representative FACS plots showing %Oct4:GFP+ cells in reprogramming hematopoietic progenitors, sampled at daily intervals. CD45 marks all hematopoietic cells. The same conditions were used for protein fractionation as shown in Fig.1b. **e** Assessing endogenous and exogenous nuclear actin by relative band intensity. Immunoprecipitation with FLAG antibody followed by western blot showed 25-fold enrichment; however, the pulldown only accounts for about a quarter of the nuclear input, suggesting overexpression to be ~1% of that of the endogenous β-actin. **f** FLAG IF in MEFs transduced with polymerization defective mutant NLS-actin^{G13R} or depolymerization defective mutant NLS-actin^{S14C}. Similar to Fig. 1d. **g-i** Hematopoietic progenitors were transduced with EV or NLS-actin constructs and induce by Dox for reprogramming. **(g)** Representative images of bright field and Oct4:GFP overlay on day 5. **(h)** Oct4:GFP histogram on day 4 and day 6. **(i)** MFI of Oct4:GFP on day 6.

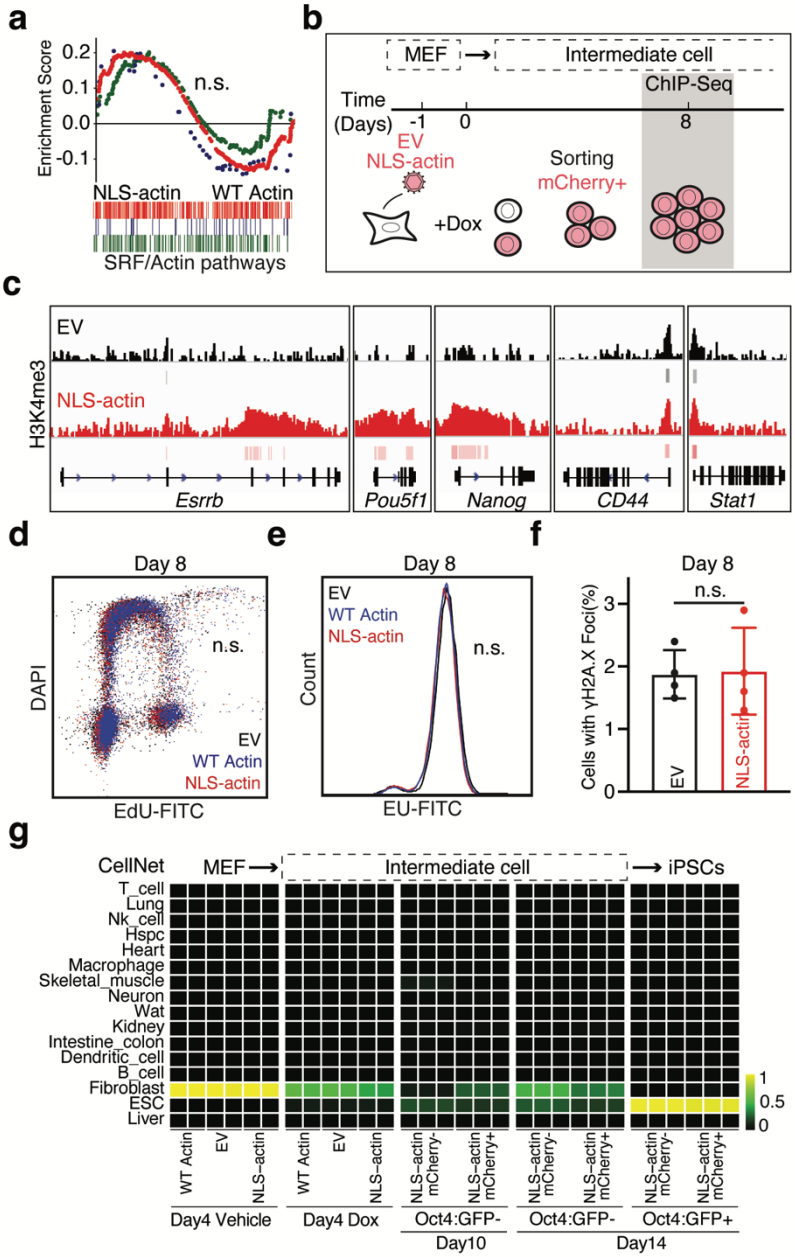

Fig. S2. NLS-actin promotes somatic cell reprogramming defying known mechanisms. a GSEA detected no difference in SRF target genes between cells expressing WT actin and NLS-actin. n.s.: non-significant. **b** Experimental scheme for cell harvesting for H3K4me3 ChIP-seq on day 8. **c** H3K4me3 binding at three representative pluripotency genes, *Esrrb*, *Pou5f1* and *Nanog*, and two fibroblast genes, *CD44* and *Stat1*. **d** Representative FACS plots of EdU labeling newly synthesized DNA, with DAPI staining all DNA. **e** Representative FACS plots of EU staining newly transcribed RNA. **f** Quantification of γH2AX foci in EV and NLS-actin transduced reprogrammable MEFs on day 8. For d-f, all experiments were performed in biological triplicates or quadruplicates and no difference was detected. **g** Full CellNet analysis with more reference cell types as in Fig. 2k.

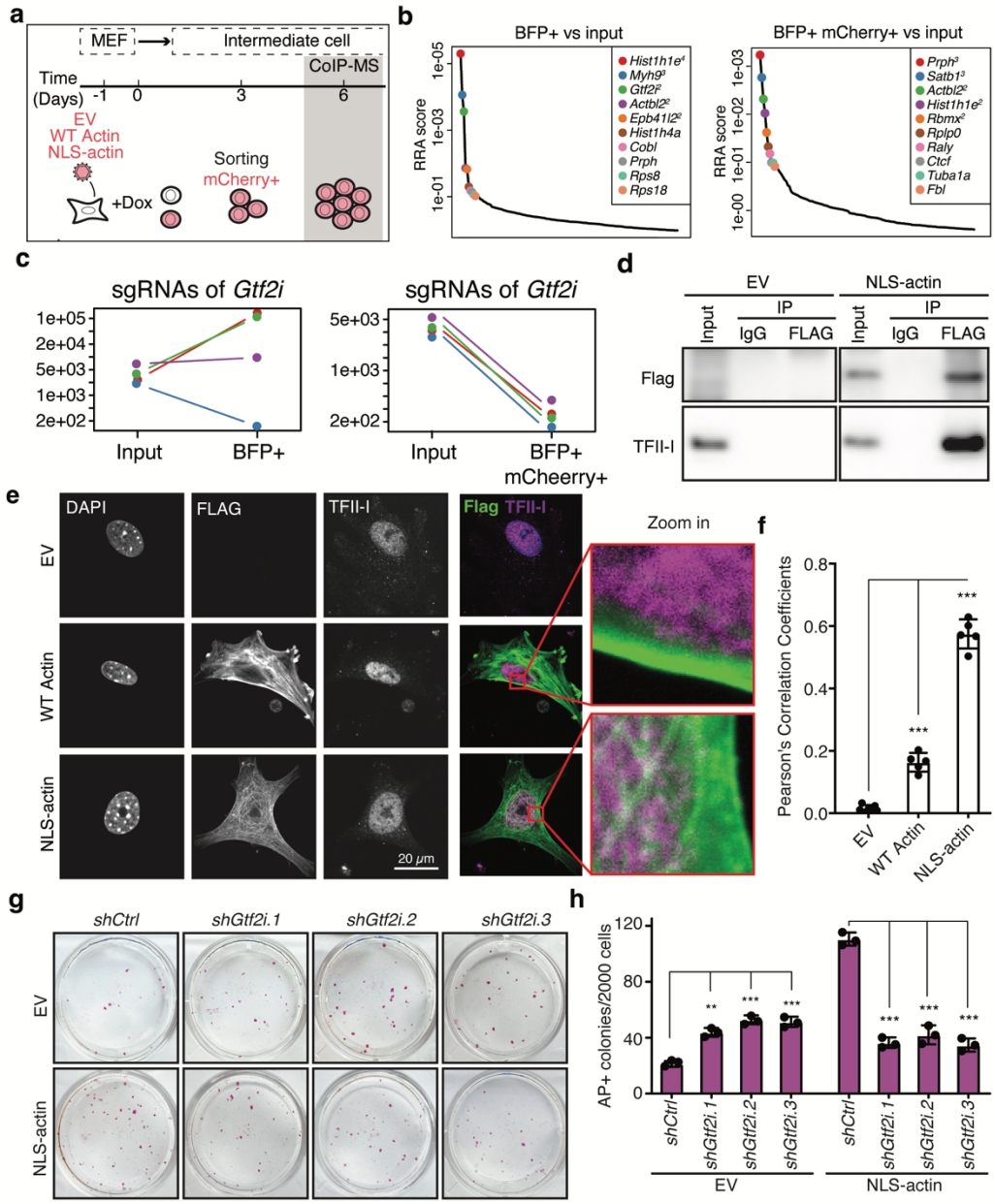

Fig. S3. *Gtf2i*/TFII-I is required for NLS-actin to promote reprogramming. **a** Experimental scheme for harvesting proteins for co-IP followed by mass spectrometry. Reprogrammable MEF expressing EV, WT actin or NLS-actin were reprogrammed for 6 days. Nuclear protein fractions from mCherry+ cells were precipitated by FLAG antibody. **b** FluteRRA (robust ranking aggregation, RRA) analysis of gRNA reads, related to Fig. 3d-e. The top 10 genes with the most gRNA counts in BFP+ cells (**left**) or BFP+/mCherry+ cells (**right**) relative to input. **c** Absolute reads number of the four individual gRNAs targeting *Gtf2i* in BFP+ cells (**left**) or BFP+/mCherry+ cells (**right**). **d** FLAG antibody pulled down endogenous TFII-I in NLS-actin but not in EV control cells. **e** Representative IF images of FLAG and TFII-I. Inset: zoom in regions across a nuclear boundary region. **f** Quantification of FLAG and TFII-I signal colocalization by Pearson correlation. n=5, ***$p < 0.001$. **g** Representative AP+ colonies on day 10 from EV or NLS-actin expressing cells with three individual shRNAs targeting *Gtf2i*. **h** Quantification of AP+ colonies in g, n=3, ***$p < 0.001$.

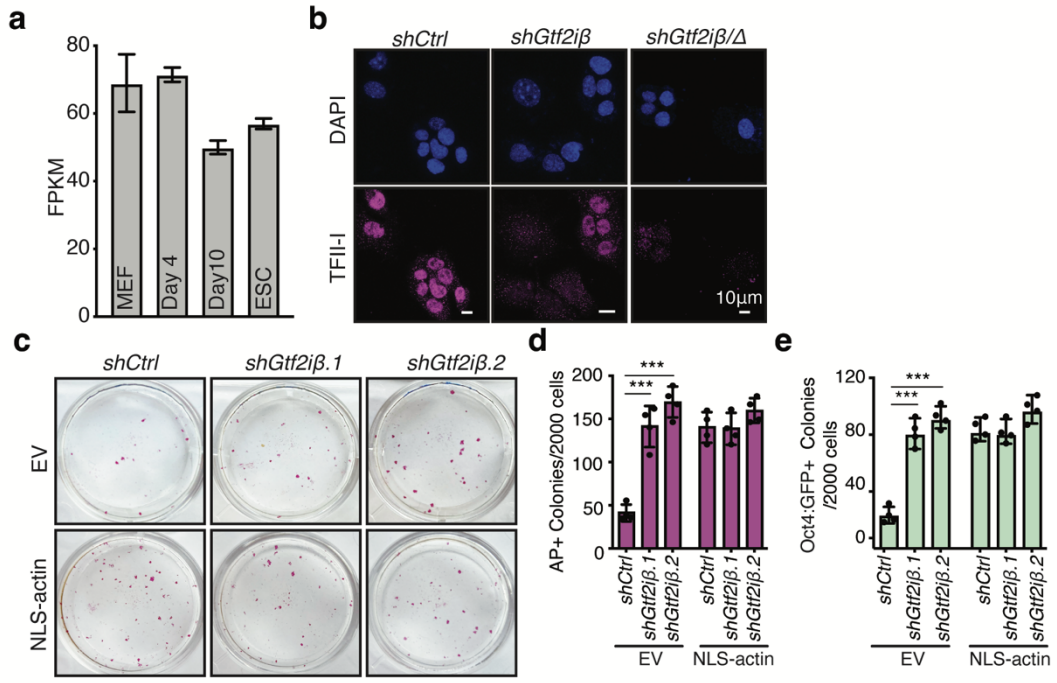

Fig. S4 The delta isoform of Gtf2i, TFII-IΔ, mediates NLS-actin's pro-reprogramming effect. a Total FPKM mapping to *Gtf2i* in various cell types. **b** IF staining of TFII-I in day 7 reprogramming cultures in the presence of shRNAs. **c** Representative AP+ colonies formed in EV or NLS-actin expressing cells in the presence of β-specific or β/Δ dual targeting shRNAs on day 10. **d** Quantification of AP+ colonies shown in c. n=4. **e** Quantification of Oct4:GFP+ colonies shown in c. n=4.

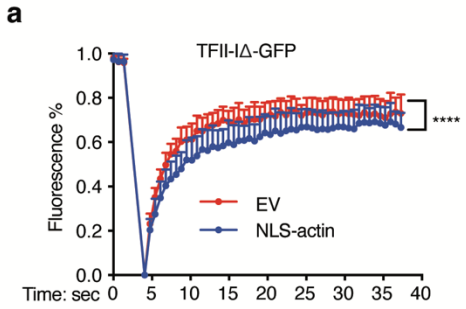

Fig. S5. Mobility of TFII-IΔ is reduced by NLS-actin expression. a FRAP analysis of TFII-I-Δ-GFP in cells expressing EV or NLS-actin. n=20 each.

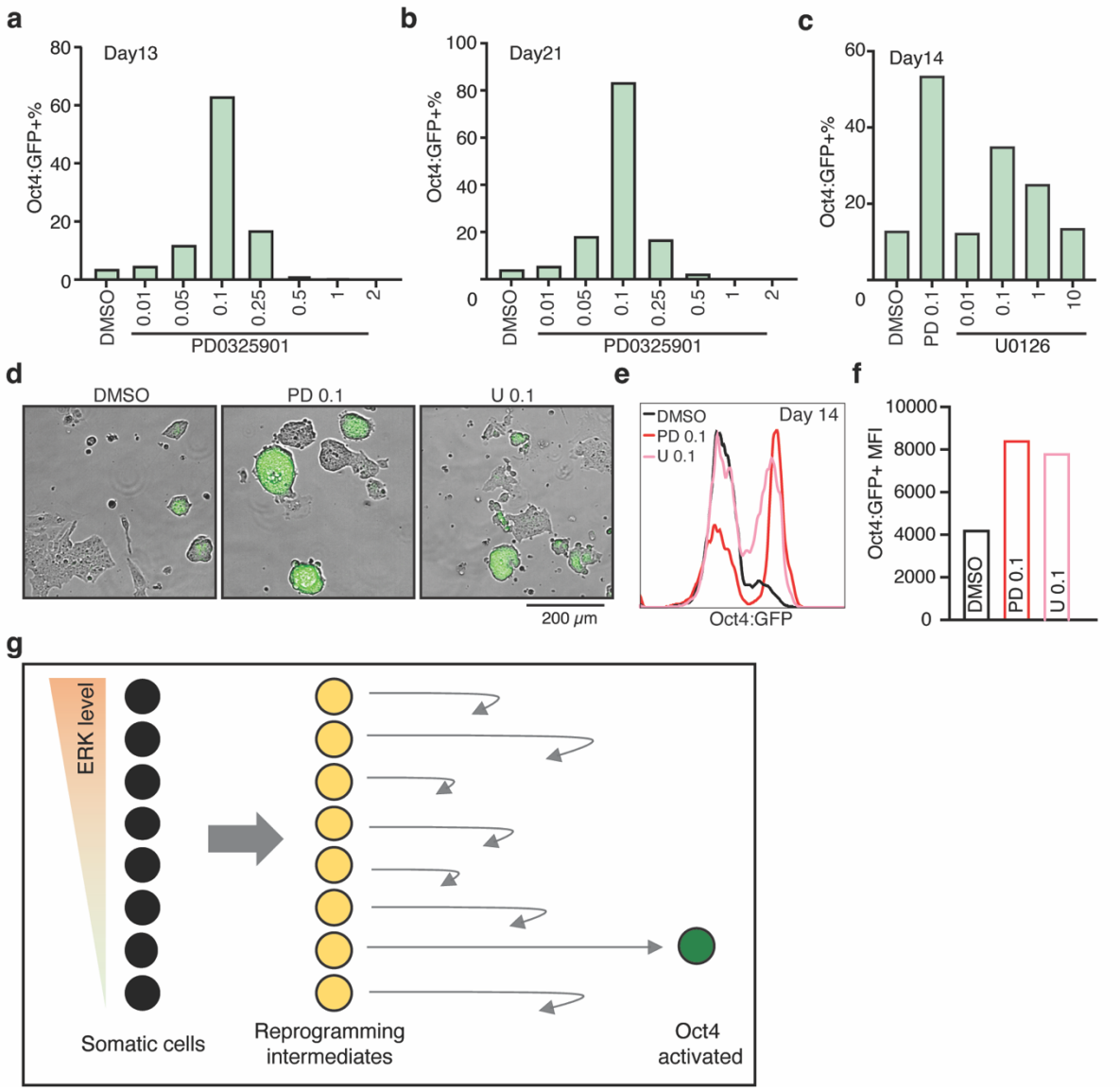

Fig. S6. Mild ERK inhibition by chemical inhibitors promotes reprogramming from most fibroblasts. a %Oct4:GFP+ cells in reprogramming cultures treated with different concentrations of PD0325901 on day 13, as shown in Fig. 6a. **b** %Oct4:GFP+ on day 21, as shown in Fig. 6a. **c** %Oct4:GFP+ in reprogramming cultures treated with different concentrations of U0126 on day 14, with 0.1μM PD0325901 as a positive control. **d** Representative bright field and Oct4:GFP fluorescence images on day 15, in the presence of 0.1μM PD0325901 or U0126, as compared to DMSO. **e** Oct4:GFP FACS for cells in d on day14. **f** Oct4:GFP MFI for cells in e. **g** Model depicting the apparent low reprogramming efficiency as gated by a low and narrow ERK activity range.

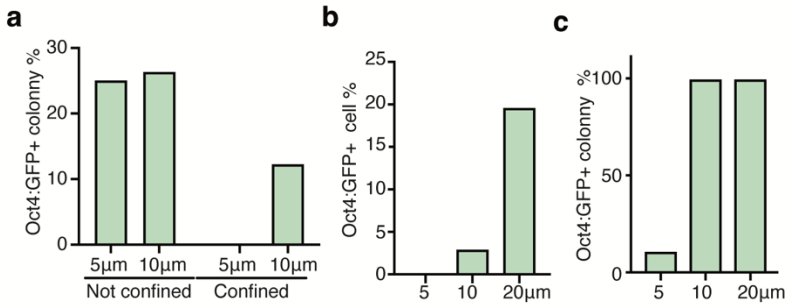

Fig. S7 Actin fails to accumulate in the nucleus below a threshold nuclear height. a Quantification of %Oct4:GFP+ colonies under 5 or 10 µm confinement, as shown in Fig. 7b. **b** Quantification of %Oct4:GFP+ cells under 5, 10 or 20 µm confinement, as shown in Fig. 7c. **c** Quantification of %Oct4:GFP+ ESC colonies under 5, 10 or 20 µm confinement, as shown in Fig. 7g.

Supplemental tables and movies

Supplementary Table 1: FPKM of all genes by RNA-seq and differentially expressed genes (DEGs) in pair-wise comparisons.
Supplementary Table 2: GO molecular function enrichment for the up- and down-regulated DEGs between cells expressing WT actin and NLS-actin on day 4 of reprogramming.
Supplementary Table 3: Annotated protein interactome of nuclear actin.
Supplementary Table 4: The NAIT library screen.
Supplementary Table 5: List of primers, shRNAs and antibodies

Movie S1. Z-stack of FLAG tagged NLS-actin, related to Fig.1d.
Images were acquired on Leica SP5 microscope at 63x, zoom in 8-fold. The movie is played from cell bottom to top at 0.38 µm steps. A total of 26 z-planes were acquired. Total z-depth is 9.44 µm.

Movie S2. Z-stack of FLAG tagged NLS-actin^{G13R}, related to Fig.S1f.
Images were acquired on Leica SP5 microscope at 63x, zoom in 8-fold. The movie is played from cell bottom to top at 0.38 µm steps. A total of 15 z-planes were acquired. Total z-depth is 5.29 µm.

Movie S3. Z-stack of FLAG tagged NLS-actin^{S14C}, related to Fig.S1f.
Images were acquired on Leica SP5 microscope at 63x, zoom in 8-fold. The movie is played from cell bottom to top at 0.38 µm steps. A total of 17 z-planes were acquired, Total z-depth is 6.04 µm.

Movie S4. Z-stack of DAPI stained reprogramming culture on day 7, related to Fig 7i.
A representative cell cluster and a fibroblast-like cell in the same field of view. Images were acquired on Leica SP5 microscope at 63x, zoomed in 2-fold. A total of 19 z-planes were acquired, at 1 µm steps. Total z-depth is 18.13µm.